THE IGNITION OF SOLID PROPELLANTS BY RADIATIVE, CONVECTIVE AND CHEMICAL HEATING

Sami Atallah, et al

Little (Arthur D.), Incorporated
Cambridge, Massachusetts

November 1969

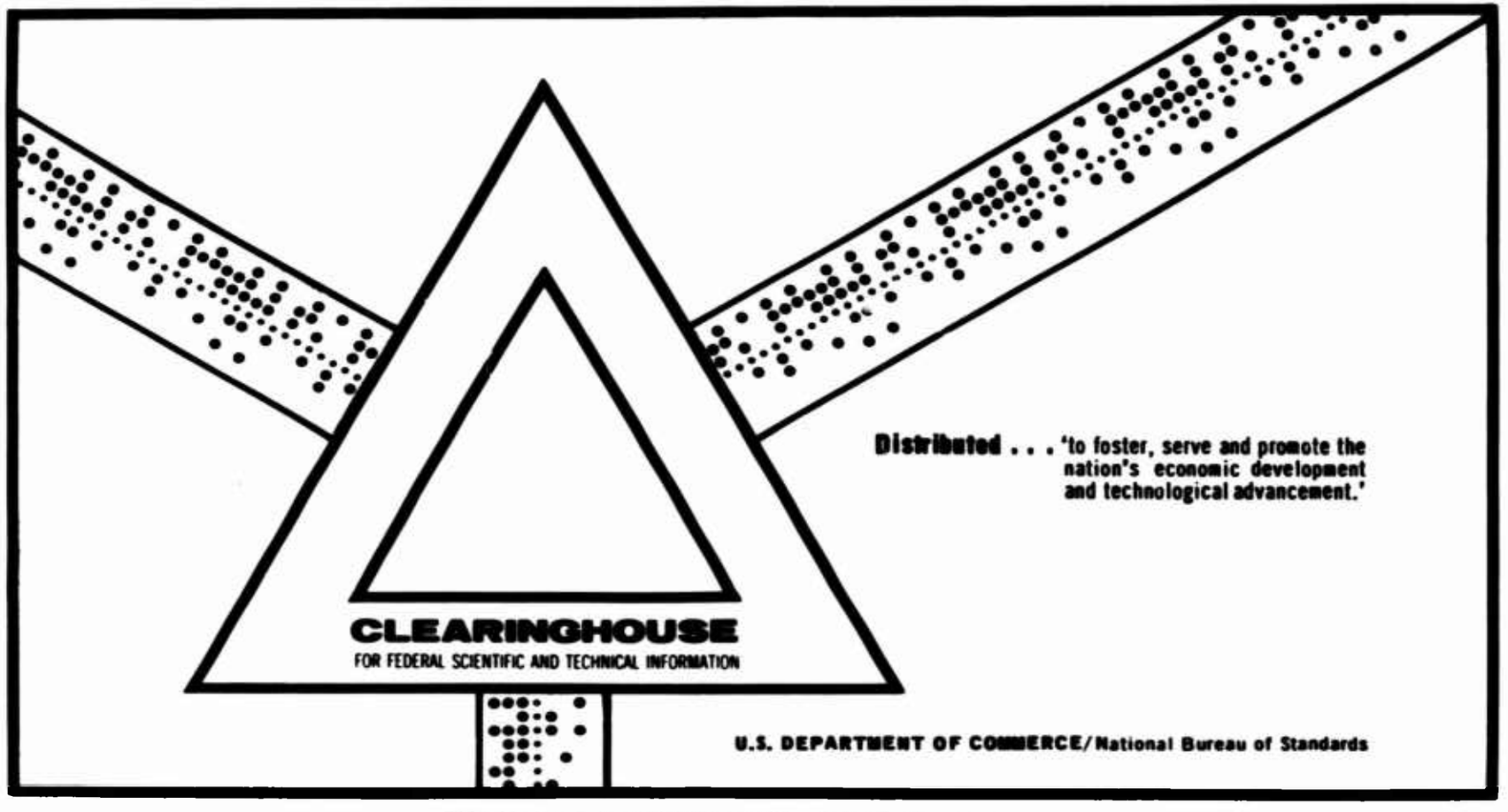

AFOSR Final Scientific Report

AFOSR 69-3091TR

THE IGNITION OF SOLID PROPELLANTS BY RADIATIVE, CONVECTIVE AND CHEMICAL HEATING

Final Report

Contract F44620-67-C-0002

Project No. 9711-01

NOVEMBER 1969

Prepared for

AIR FORCE OFFICE OF SCIENTIFIC REREARCH
OFFICE OF AEROSPACE RESEARCH
UNITED STATES AIR FORCE

68727

1. This document has been approved for public release and sale; its distribution is unlimited.

Arthur D. Little, Inc.

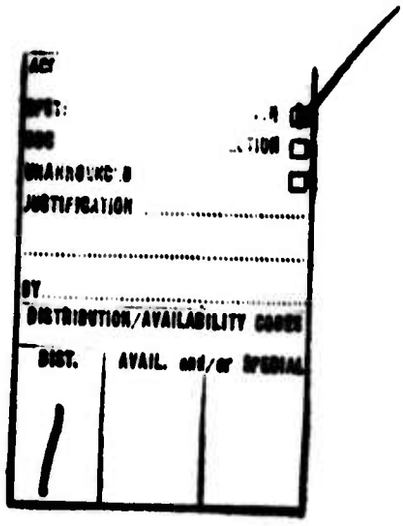

THE IGNITION OF SOLID PROPELLANTS BY RADIATIVE, CONVECTIVE AND CHEMICAL HEATING

Final Report

S. Atallah, D. S. Allan, D. F. Comstock Jr., and B. H. Bakerjian

Contract F44620-67-C-0002

Project No. 9711-01

November 1969

Research Sponsored by

Air Force Office of Scientific Research
Office of Aerospace Research
United States Air Force

Submitted by

Arthur D. Little, Inc.
Cambridge, Massachusetts 02140

68727

1. This document has been approved for public release and sale; its distribution is unlimited.

FOREWORD

This program was sponsored by the Air Force Office of Scientific Research and monitored by Dr. Bernard T. Wolfson and Colonel Richard W. Haffner of the Directorate of Engineering Sciences. The program was initiated in 1966 with E. Karl Bastress as Principal Investigator. Donald S. Allan became Principal Investigator when Dr. Bastress left Arthur D. Little, Inc., in 1967.

The authors wish to acknowledge the assistance of Messrs. C. D. DiFraia and J. Cleary in constructing the fluorine apparatus and in the conduct of the tests.

ABSTRACT

This report presents the results of an experimental study in which aluminized and non-aluminized composite solid propellants were ignited under different environmental conditions. Ignition was achieved by radiative, convective and chemical heating. An optical system operating in two narrow wavelength bands was used to detect the onset of ignition on and near the surface of the propellant. It was found that ignition delay time was dependent on the wavelength used for detection, the method of heating, and other environmental factors. The implications of these results are discussed in relation to existing ignition theories, and recommendations are made for further study.

NOMENCLATURE

a	area of the sample (cm^2)
A	preexponential constant
B	preexponential constant
c_1	Planck's first constant
c_2	Planck's second constant
C_o	concentration of oxidizing species (gm/cc)
C_p	specific heat (cal/gm °C)
E	activation energy (cal/gm)
E_s	activation energy (cal/g-mole)
k	thermal conductivity (cal/cm sec °C)
n	order of reaction
P	pressure (atm)
P_λ	spectral flux (watt/μM steradian)
$\dot{q}$	heat flux (cal/cm^2 sec)
Q	heat of reaction
r	rate of reaction at T
r_{ig}	rate of reaction at T_{ig}
r_o	rate of reaction in an inert atmosphere
R	universal gas constant (cal/g-mole °K)
S	slope of log $\tau^{1/2}$ vs log $\dot{q}$
T	temperature (°K)
T_{ig}	ignition temperature (°K)
T_o	initial temperature (°K)
T_s	surface temperature at steady combustion (°K)
x	distance (cm)
Z	Arrhenius preexponential factor

Greek Letters

α	thermal diffusivity (cm^2/sec)
β	solid angle for sample emission collected by optical detector (steradian)
ε_λ	spectral emittance

NOMENCLATURE - Cont'd.

λ	wavelength (μM)
ρ	density (gm/cc)
T	transmittance of the optical system
τ	ignition delay time (sec)

TABLE OF CONTENTS

TABLE OF CONTENTS (CONT'D)

LIST OF FIGURES

LIST OF FIGURES (CONT'D)

LIST OF TABLES

I. SUMMARY

This report describes recent experimental studies performed at Arthur D. Little, Inc., with the objective of arriving at a better understanding of solid propellants ignition mechanisms.

An arc-imaging furnace, a hot gas tunnel and a fluorine gas system were used to provide radiative, convective, and chemical energy for the ignition of an aluminized and a non-aluminized composite PBAA/AP propellant. The ignition process was observed by a unique optical system which allowed the simultaneous detection of emission in two regions of the spectrum. Radiation from a small circular spot on the propellant surface was collected, split and passed through two narrow wavelength interference filters. A lead selenide cell was used to detect infrared radiation at a wavelength of 3.79 μM which was selected as being virtually free from interfering CO_2, H_2O and other flame line and band emission (except for particulate matter) and thus represented radiation from the propellant surface. A photomultiplier was used to detect the CH radical from the flame at .43 μM.

Ignition delays of the two propellants subjected to different heating modes and environmental conditions were compared with theoretical predictions and with each other. It was found that the non-aluminized propellant had greater ignition delays when heated radiatively than the aluminized propellant but smaller delays when ignited convectively. The presence of excess oxygen in the hot gases which were used to heat the propellant by convection decreased ignition delay. Chemical heating with fluorine produced the shortest ignition delay.

Differences were observed in ignition delay time as measured by the detectors operating at the two wavelengths. These differences were most pronounced when ignition was achieved by convective heating and indicated the occurrence of exothermic reactions on the surface before ignition took place in the gas phase.

The results were used to recommend further avenues for research. Propellant test procedures and ignition delay detection systems need to be reevaluated and standard techniques developed if valid comparisons between the results of different investigators are to be made.

II. INTRODUCTION

2.1 Previous Studies at Arthur D. Little, Inc.

The ignition of solid propellants has been the subject of several studies at Arthur D. Little, Inc. The general objective of these previous studies has been to understand the mechanisms of solid propellants ignition when subjected to radiative, convective or chemical heating. This necessitated the design and construction of equipment and instruments to facilitate the observation of the ignition process.

In the previous work, an arc-imaging furnace was used to study ignition under radiant heating conditions.[1] Methods were developed for determining propellant ignition time by direct observation of the sample during continuous exposure to radiation. The effects of flux intensity and spectral distribution on ignition were observed using broad band photo-detectors.

A convective heating apparatus was also developed which utilized mixtures of combustible gases to provide realistic ignition conditions similar to those occurring in rocket motors. Effects of gas pressure, temperature, velocity, composition, and solid particle content on propellant ignition delay time were found,[2,3] again using broad band photo-detectors and cinephotography.

Further studies were conducted in this apparatus with elongated samples.[4] The approach material, gas velocity, and test chamber configuration were varied and their effect on ignition delay time was also found.

A theoretical analysis was also conducted of the combined effects of radiation, pure convection, vapor condensation, and shifting composition on the total transfer of energy from igniter products to a cool surface.[5] This analysis utilized an ethalpy rather than temperature driving force, and a relatively simple film model of heat transfer was developed which has proved to be useful in the analysis of experimental data.

2.2 Objectives of the Present Studies

Throughout this prior work, better techniques were sought for detecting the onset of ignition of the propellant sample. Our early studies had shown that wide band photo-detectors operating in the IR region of the spectrum detected a sudden rise in signal with corresponding temperatures that were unexpected from the surface heating of a semi-infinite solid. This event preceded ignition as indicated by a photo-cell which responded to visible light and it gave rise to uncertainty as to when ignition actually occurred. In the past, the point of ignition had been arbitrarily chosen as when sufficient light was given off to be detected by a photosensitive detector. This criterion was relatively easy to use to determine when ignition occurred with aluminized propellants since they emitted a large quantity of light upon ignition. However, in the case of non-aluminized propellants, there was no abrupt change in the output of the photosensitive detector during the ignition process. Furthermore, with both aluminized and non-aluminized propellants, there was evidence that gases were evolved from the propellant surface for a considerable period of time prior to the detection of light with the photosensitive detector. Others had reported similar difficulties in determining the exact onset of ignition.

It was thus desired to devise a system by which the details of the thermal processes occurring during ignition could be observed. An optical detector which could respond to thermal radiation from the propellant surface and to visible radiation from the flame simultaneously and independently was an obvious solution. Such a detector could then be utilized to compare the ignition behavior during radiative, convective and chemical heating under varied environmental conditions. It could also be used to measure the surface temperature during the ignition process. The results were to be used to arrive at a better understanding of propellant ignition mechanisms.

2.3 Theories of Ignition

This section is intended as a summary of the different theories proposed for propellant ignition for easier reference within this report. It is not intended to supersede the excellent classical reviews of Price et al[6] and Brown et al[7].

2.3.1 Thermal Ignition Theory

This theory assumes that ignition occurs when the propellant surface temperature is such that the rate of heat generated by surface reactions is high enough for the reaction to be self-sustaining. The unsteady heat flow into a homogeneous semi-infinite propellant is described by the equation[8]

$$\frac{\partial T}{\partial \tau} = \frac{\partial^2 T}{\partial x^2} + BQ\exp\ (-E/RT) \qquad (2.1)$$

and the appropriate boundary conditions. If it is further assumed that the solid is opaque and inert, that heat flux at the surface and the thermal properties of the propellant are all constant and that ignition takes place when the surface temperature reaches a unique value, T_{ig}, Equation (2.1) can be solved[9] to give

$$T_{ig} - T_o = \frac{2\dot{q}}{k}\left(\frac{\alpha \tau}{\pi}\right)^{1/2} \qquad (2.2)$$

This equation suggests that for a given propellant, a plot of log τ vs log $\dot{q}$ should give a line with a slope of -2. Other forms of plotting this equation such as $q(=\dot{q}\tau)$ vs. $\dot{q}$ and $\tau^{1/2}$ vs. $\dot{q}$ had been suggested and used. Numerical solutions of Equation (2.1) by Baer and Ryan[10] showed that the slopes of log $\tau^{1/2}$ vs. log $\dot{q}$ can be used to obtain the activation energy of the propellant surface reaction by the approximate relation.

$$S = 4.2\ \frac{RT_o}{E} - 1 \qquad (2.3)$$

Deviations in the behavior of a propellant from Equation (2.2) can then be attributed to chemical heat release on the surface, the translucency of some propellants to thermal radiation, heat losses to the surrounding gas if it is cooler than the surface, and to chemical reaction of the surrounding oxidizing atmosphere (if present) with the solid propellant or with its decomposition products. The thermal ignition theory does not provide for pressure effects on ignition delay and its applicability to composite propellants has been questioned.

2.3.2 Gas-Phase Ignition Theory[11]

This theory assumes that the ignition reaction takes place in the gaseous phase between the pyrolysis products of the propellant. In this case, gas reaction kinetics and diffusion rates of species are included in the analysis. The complicated mathematical treatment of this mechanism is far from being complete and is not in a form which can be easily related to experimental data.

2.3.2 Heterogeneous Ignition Theory

This theory assumes that reactions can take place between the polymer and the oxidizing gases generated by the decomposition of the oxidizing component of the propellant. An energy balance at the surface is given by

$$-k \frac{\partial T}{\partial x} = \dot{q} + Z\, C_o(P)\, \exp(-E_s/RT) \qquad (2.4)$$

Thus the effect of pressure on ignition delay which was lacking in Equation (2.1) is included here. Beyer[12] used Equation (2.4) as a boundary condition for Equation (2.1) and arrived at a semi-theoretical correlation between delay time, heat flux and pressure.

$$\tau = \left[\frac{d^3}{\dot{q}^6} + \frac{b^3}{p^{6.45}} \right]^{1/3} \qquad (2.5)$$

For large P and small $\dot{q}$, (i.e., when $\frac{d\, P^{2.15}}{\dot{q}^2} >> b$), Equation (2.5) becomes

$$\tau \simeq d\, \dot{q}^{-2}$$

which is similar to Equation (2.2).

Beyer showed that he could correlate ignition delay times at different pressures and fluxes by plotting $\tau\, P^{2.15}$ vs. $\dot{q}/P^{1.0}$.

2.3.4 Ignition by Chemical Heating (Hypergolic Ignition)

When a very reactive oxidant such as fluorine or ClF_3 contacts the surface of a propellant, a heterogeneous exothermic reaction occurs between the oxidant and the solid phase. The heat generated at the surface raises the solid to its ignition temperature very quickly. Anderson et al[13] analyzed this system and showed that if the activation energy is very small

$$\tau \propto \frac{1}{C_o^{2n}} \qquad (2.6)$$

where C_o is the oxidizer concentration and n is the order of the surface reaction.

III. THE OPTICAL DETECTION SYSTEM

To observe the thermal processes occurring on and near the surface of a propellant during ignition, it was desired to design and construct an instrument which could respond to electromagnetic radiation from the propellant surface and from the gases above the surface simultaneously and independently. This chapter describes the criteria used in designing this unique detection system, its method of operation and calibration and its limitations.

3.1 General Requirements and Constraints

Four major criteria were considered in selecting a suitable electromagnetic radiation method. These were:

- Cooling requirements
- Signal-to-noise ratio
- Spectral selectivity, and
- Speed of response

Because of the nature and variety of the planned ignition tests, it was practical to eliminate detection systems requiring cryogenic cooling and to employ one that would operate at ambient temperature.

Electromagnetic radiation detection methods always detect a certain minimum level of noise (e.g., current noise, Johnson noise, or background radiation noise, depending on the detector and amplifier). The detection noise level, whatever its cause, obscures signals smaller than a certain minimum level. In terms of temperature, the noise level in the system corresponds to and limits measurements to a certain minimum detectable temperature. The instrument was to be designed so that noise could be reduced and the minimum measurable temperature lowered by careful choice of detector and collection optics and by beam chopping combined with electronic frequency discrimination.

Spectral selectivity could be used to discriminate between individual events during ignition by the use of separate narrow spectral bands each responding to a different source of emission within the ignition region. However, although spectral selectivity increases with narrowing spectral bandwidth, infrared signal and signal-to-noise ratio (with an uncooled

detector) decrease with narrowing spectral bandwidth. Thus, selectivity must be balanced against the desired strength of the signal and the acceptable minimum detectable temperature.

Speed of response, in general, is not limited by the detector, but by the repetition period of the beam chopper. Discrimination against noise by chopping and electronic frequency discrimination has the effect of transmitting the signal in the form of a frequency band carrier modulated by the ignition signal. Events occurring within a period of time shorter than one cycle (the time between chops) cannot be resolved; and therefore, the chop period defines the minimum resolvable time of the instrument.

3.2 Features of Total and Spectral Radiation Methods

There were a number of possible choices among optical methods involving broad and narrow wavelength bands and the position of the band. One common feature among these methods was the need for focusing radiation from a small region in which the ignition event took place onto the detection system.

Total radiation as described by the Stefan-Boltzmann law provides a straightforward basis for the measurement of temperature and is perhaps the most sensitive since virtually all of the radiation from the observed region which enters the detector aperture is utilized. At sample temperatures occurring during the heating phase just prior to the onset of ignition, the total radiation method offers the most favorable signal-to-noise ratio and is capable of resolving the lowest minimum detectable sample temperature. Such a broad wavelength band detector had been used in our previous studies.[1] This type of detector, however, cannot be used to differentiate between events taking place on the surface and in the gases near the surface.

Monochromatic radiation provides a second basis for the measurement of temperature and has certain advantages. Planck's law rearranged and expressed in terms of instrument filter bandwidth is:

$$P_\lambda = \frac{\epsilon_\lambda c_1 \lambda^{-5} \Delta\lambda \beta T a}{\left(e^{c_2/\lambda T} - 1\right)} \qquad (3.1)$$

or

$$T = \frac{c_2}{\lambda \ln\left[c_1 \left(\beta T a\right)\left(\frac{\Delta\lambda}{\lambda^5}\right)\left(\frac{\epsilon_\lambda}{P_\lambda}\right) + 1\right]} \qquad (3.2)$$

where

P_λ is the spectral flux delivered to the detector emitted from and normal to the sample face (watt/ M steradian)

ϵ_λ is the spectral emittance of the sample surface or a term combining several factors to represent flame emission

c_1 is Planck's first constant

c_2 is Planck's second constant

T is the sample surface temperature (°K)

λ is the wavelength of detection (μM)

$\Delta\lambda$ is the wavelength band of detection (μM)

β is the solid angle of sample emission collected by the detection optics (steradians)

T is the transmittance of the optics

a is the area observed on the sample defined by an aperture in an image plane (cm^2).

The spectral flux emitted from the sample and delivered to the detector as represented by Equations (3.1) or (3.2) is proportional to the signal received by the detector and provides a means for determining sample temperature.

The wavelength, λ, can be any chosen value convenient for pyrometry and will indicate the same sample temperature, regardless of its value, providing that the sample emittance and instrument terms in Equation (3.2) are correctly evaluated at the chosen wavelength. However, the instrument terms β, T, and a cannot be easily evaluated (at a given wavelength) individually and absolutely but they can be collectively eliminated by using a calibration source. Equation (3.1) can then be written once for the calibration source and again for the sample and the ratio taken and rearranged to give an equation free of instrument terms:

$$T_s = \frac{c_2}{\left[\lambda \ln\left(\frac{P_c}{P_s}\right)\left(\frac{\varepsilon_s}{\varepsilon_c}\right)\left(\frac{\Delta\lambda_s}{\Delta\lambda_c}\right)\left(e^{c_2/\lambda T_c} - 1\right) + 1\right]} \qquad (3.3)$$

where subscript c indicates the calibration source and subscript s indicates the sample.

3.3 Choice of Operating Wavelengths

The fact that any wavelength could be chosen for monochromatic pyrometry offered the possibility of selecting particular wavelengths which would respond to or emphasize different mechanisms of emission. To observe the flame and solid surface temperatures as a function of time during ignition, separate measurements were needed which could be made by the choice of two appropriate wavelengths for detection. Furthermore, by splitting the radiant beam from the propellant, the measurement of the two temperatures could be made simultaneously and independently.

A wavelength of .4310 μM was chosen to observe the thermal processes occurring in the flame. This line is emitted by the CH radical in the flame and is reasonably intense, relatively free from overlap from other sources and an interference filter at this wavelength was commercially available. Since the absolute magnitude of the flame temperature was not as significant to this study as the point when there was an unusual increase in the signal due to CH radical generation in the gases near the surface, an approximate value of .01 was used to substitute for the term, $\varepsilon_s \Delta\lambda_s/\Delta\lambda_c$ in Equation (3.3). It was estimated that maximum errors in the calculated flame temperature were about $\pm$ 300°K.

To observe the thermal processes in the solid surface, it was desired to find an infrared wavelength window in the flame through which radiation from the surface could pass without interference. The flame gases which have absorption bands in the infrared region consisted mainly of CO_2 and H_2O. It was found that a wavelength of 3.79 μM provided a wavelength window which was virtually free from gaseous emission

and was thus chosen for observing the solid surface during heating.

3.4 Description of the Optical Detection System

A dual wavelength optical-measuring instrument was thus designed and built and used on all three phases of the ignition studies described in this report.

Figure 3.1 is a schematic diagram of the instrument which consisted of collection optics, a beam splitter, two separate interference filters, two separate fast-response detectors each followed by an amplifier with variable integer gain settings, and a multichannel galvanometer recorder capable of recording events as short as a fraction of 1 millisecond. In all three phases of the ignition studies a rotating shutter wheel was inserted in an image plane to interrupt the radiation from the sample so that alternating signal frequency discrimination techniques could be used to separate radiation from the sample from reflected or background radiation, electrical noise, and dc signals arising from other sources in the system.

The optical components of the dual wavelength measuring instrument are shown in Figure 3.2. Radiation from a 1.6 millimeter spot on or near the sample surface was collected in a 9° half-angle cone by a front surface aluminized magnesium fluoride-coated toroidal mirror placed 10 inches from the sample surface. The radiation from this toroid was redirected by a flat front surface mirror to form an image of the sample at an image plane. An aperture at this image plane defined the 1.6 millimeter diameter area viewed on the sample. The rotating shutter wheel was inserted into the beam near the first image plane in the case of the radiative apparatus and near the plane of the front surface of the sample in the case of the convective and chemical apparatus. After passing through the defining aperture in the first image plane, the beam was split by an uncoated amorphous sapphire-polished plate at about 45° to the primary beam. The directly transmitted branch of the beam passed to a blackened housing containing the 3.79μM, 4%-half-power-width interference filter behind which was a lead selenide photo-resistive detector joined to an aluminum thermal sink block. The only unusual

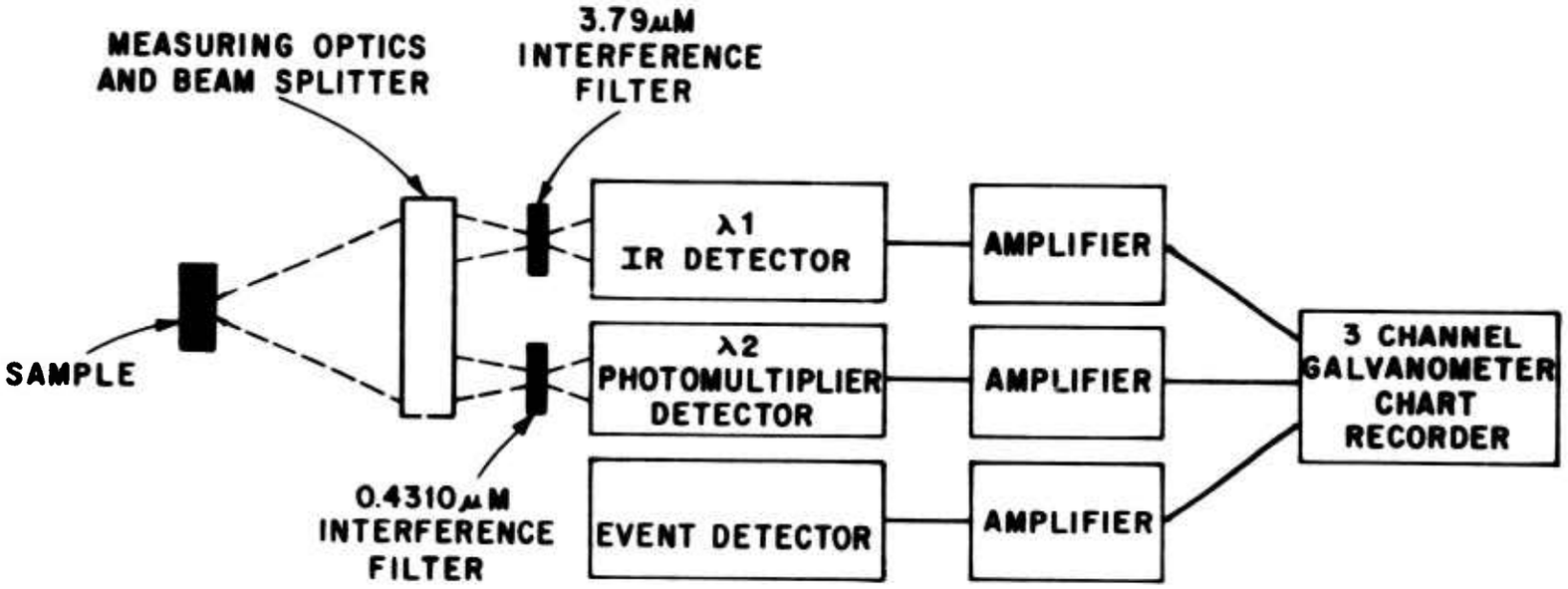

FIGURE 3.1 SCHEMATIC DIAGRAM OF THE OPTICAL DETECTION SYSTEM

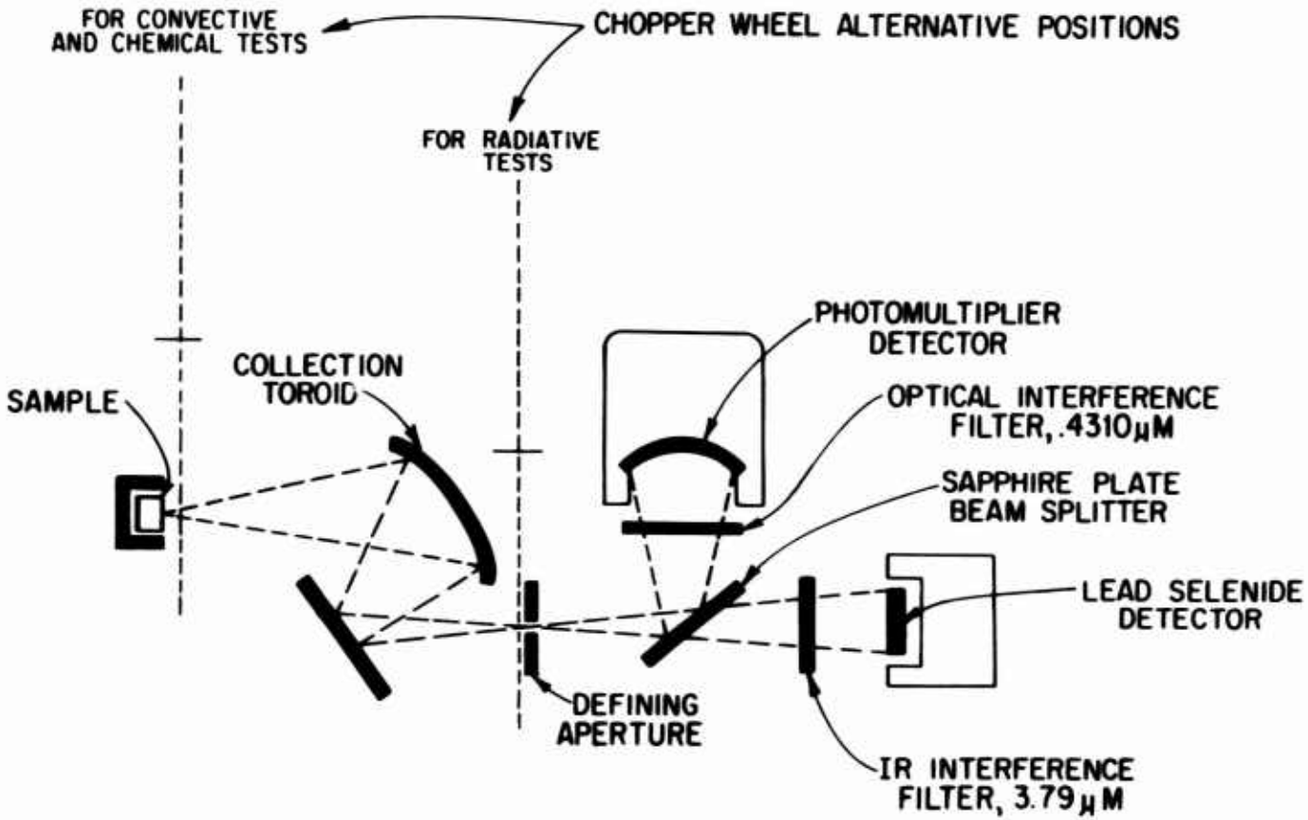

FIGURE 3.2 THE DUAL WAVELENGTH OPTICAL DETECTOR

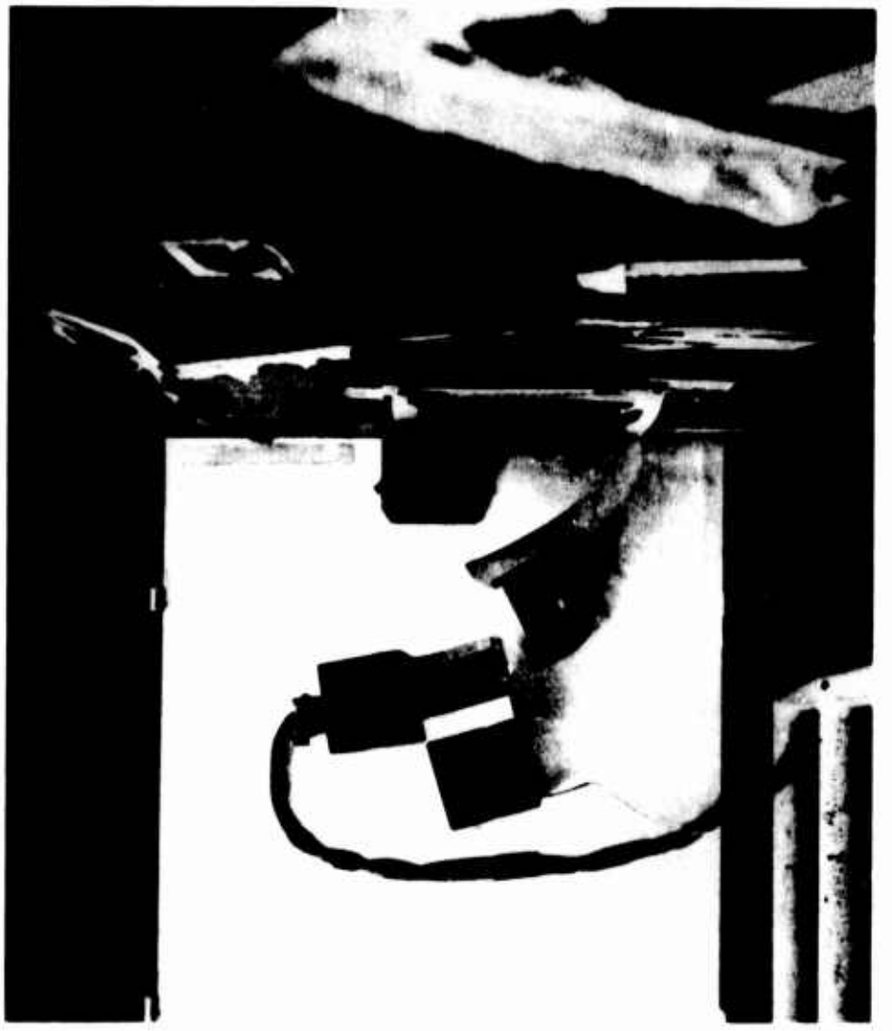

FIGURE 3.3 PHOTOGRAPH OF THE OPTICAL DETECTION SYSTEM AS USED IN THE FLUORINE APPARATUS

feature o f the amplification in the IR branch was the use of a low-noise amplifier, (Princeton Applied Research CR4 amplifier) with adjustable high- and low-frequency pass filters which were used as a tunable frequency discrimination circuit. The fresnel-reflected branch of the split beam passed to a blackened housing containing a .4310 μM, 3%-half-power width interference filter behind which was located a nine-stage photomultiplier (1P28 having S-5 spectral response).

A photograph of the dual-wavelength optical apparatus as used in connection with the chemical ignition (fluorine) apparatus is shown in Figure 3.3.

3.5 Calibration Procedure

The dual wavelentgh optical detection system was focused and properly aligned using a point light source in place of the sample. The visible image of this point source was made to pass centrally through the image defining aperature in the optical system. The beam splitter and the detectors were adjusted so that each beam fell squarely on the active area of each detector.

The interference filters were inserted in each beam, a light cover placed over the instrument, and the detector, shutter, and tuned amplifiers checked out using the chopped signal from the point source viewed on an oscilloscope.

The instrument was calibrated using two separate reference sources: one for the visible wavelength (flame) channel and one for the infrared wavelength (solid surface) channel. Each source was mounted in a holder and raised to an equilibrium temperature roughly comparable in magnitude to the expected flame or solid temperature.

The reference source for calibrating the visible (flame) detector channel was a closely wound tungsten filament lamp Philips M/16 13347C run typically at 1730°K.

The infrared (solid surface) detector channel was calibrated using a blackbody cavity made of graphite, which was electrically heated and which had gold plated water cooled baffle plates and a housing which was flushed continuously with a gentle flow of argon. This cavity provided a very uniform source of blackbody radiation adjustable from 750°K to 1100°K having a .250 inch circular aperture with spectral emittance at 3.79 micrometers of .97.

IV. PROPELLANT IGNITION BY RADIANT HEATING

4.1 Apparatus and Procedure

The ADL-Strong Arc Imaging furnace was used to provide radiant energy for the ignition of the propellants. Flux intensity was varied by the use of attenuating screens. A more detailed description of the apparatus is given in a previous publication[1]. A diagram of the apparatus including the optical detection system is shown in Figure 4.1.

The sample holder consisted of a 1 inch diameter stainless steel plug with a cavity 3/8 inch in diameter and 1/8 inch deep. The cavity was coated with epoxy glue. The propellant sample was cut with a cork borer and pressed into the cavity. The sample holder was then placed in a dessicator and the epoxy was allowed to cure overnight. Just before using the sample, a razor was used to slice the projecting portion of the propellant so that it became flush with the metal surface. The sample holder was inserted in an assembly through which gases could be passed over the surface of the propellant and the flow rate measured with a pitot tube.

After the chopper wheels and the optical detection system had been turned on and the furnace activated, a shutter was opened allowing thermal radiation to fall on the propellant surface. The chopper wheels rotated at such a rate so that the chopping cycle was 2.83 msec. Thermal radiation was allowed to fall on the surface 90% of the time while 5% of the time was used to detect surface and gas temperatures.

4.2 Test Conditions

Two types of propellants were employed throughout this study. One was a mixture of 20% PBAA - 80% AP which is referred to hereafter as the non-aluminized propellant. The other was Thiokol's aluminized PBAA/AP propellant No. TP-H-8009, Thic l Corporation - unit 587, CPIA/M2 Solid Propellant Manual.

By employing appropriate filters, heat fluxes of 8.2, 17.5, 35.1, and 53.4 cal/cm^2 sec were obtained. Argon and oxygen were allowed to flow past the sample surface at two different flow rates: 0 and 24 m/sec.

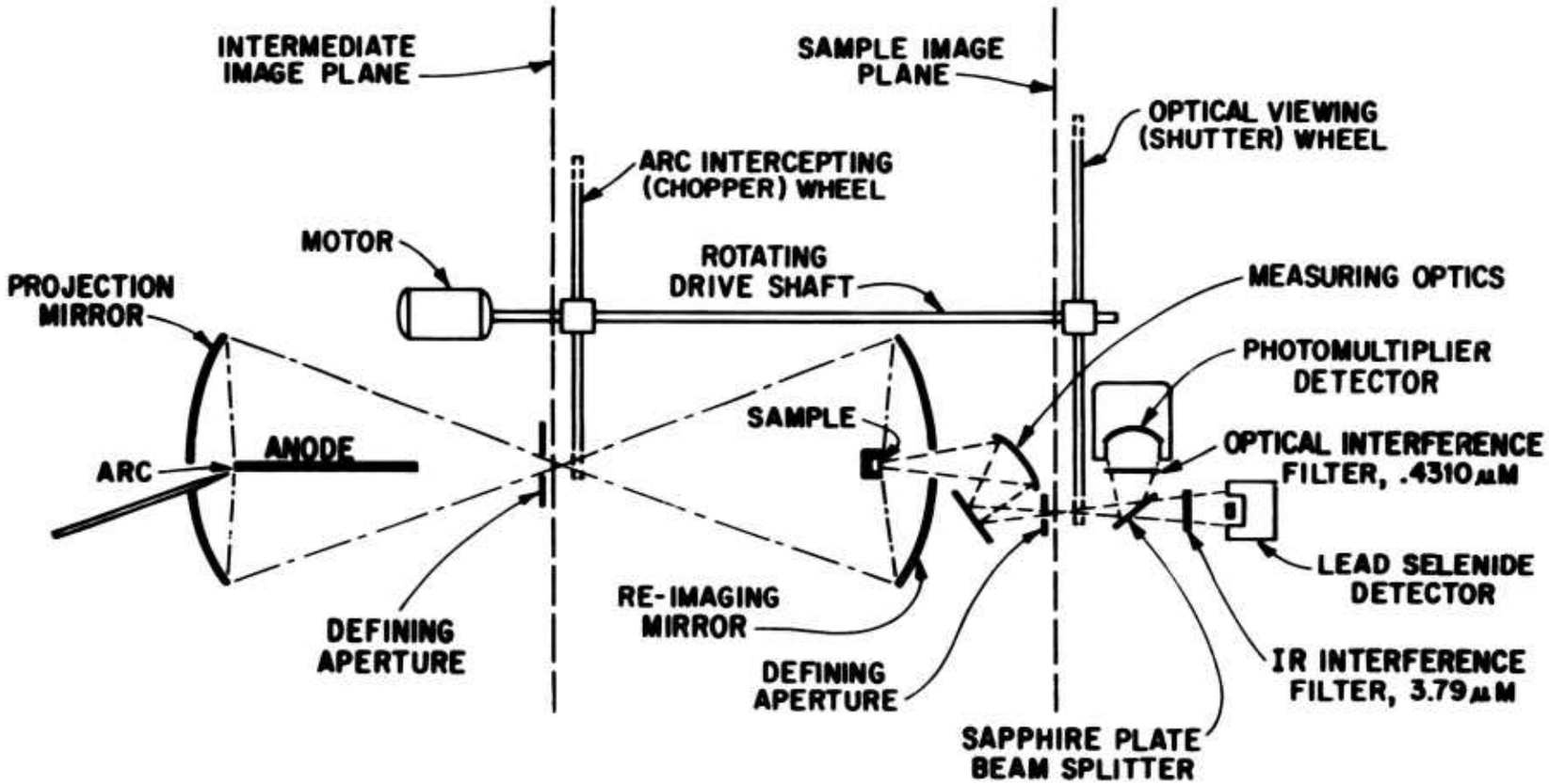

FIGURE 4.1 ARC IMAGE FURNACE AND MEASURING OPTICS

The experiments were conducted at atmospheric pressure. The sample was initially at room temperature.

4.3 Presentation of the Results

The IR visible radiation detector outputs were converted into temperature-time plots. Typical results are shown in Figures 4.2, 4.3, 4.4, and 4.5. The heating curve for an inert opaque propellant as calculated from the general form of Equation (2.2) is superimposed on the surface temperature record obtained from the IR detector output. For the purposes of this calculation, the propellant was assumed to have the following properties[1]:

$$k = 1.5 \times 10^{-3} \text{ cal cm}^{-1} \text{ sec}^{-1} \text{ °C}^{-1}$$

$$\rho = 1.7 \text{ gm cm}^{-3}$$

$$C_p = 0.3 \text{ cal gm}^{-1} \text{ °C}^{-1}$$

It was generally observed that the theoretical heating curve agreed fairly well with the experimental IR curves for the aluminized propellant (See Figures 4.2 and 4.3). There was also a sharp rise in the IR and visible radiation detector outputs at ignition. For the non-aluminized propellant, however, ignition delay was relatively longer and the ignition process more gradual so that it was difficult to define the exact time of onset of ignition from the detector output traces. (Compare Figures 4.2 and 4.3 with Figures 4.4 and 4.5). Furthermore, the theoretically predicted temperatures for an inert opaque solid were much higher than the surface temperatures measured by the IR detector.

Two definitions of ignition delay were used in the analysis. For both types of propellant, the onset of ignition was taken as the point on the visible radiation detector output where a sudden rise in temperature brought it to a point above the minimum detectable temperature (≈ 1700°K) and the time interval between initiation of heating to ignition designated τ_{vis}. Another ignition delay, τ_{ir}, was also estimated from the IR detector (surface temperature) record where ignition was assumed to have occurred when there was a noticeable increase in the rate of temperature rise. The results are tabulated in Table 4.1

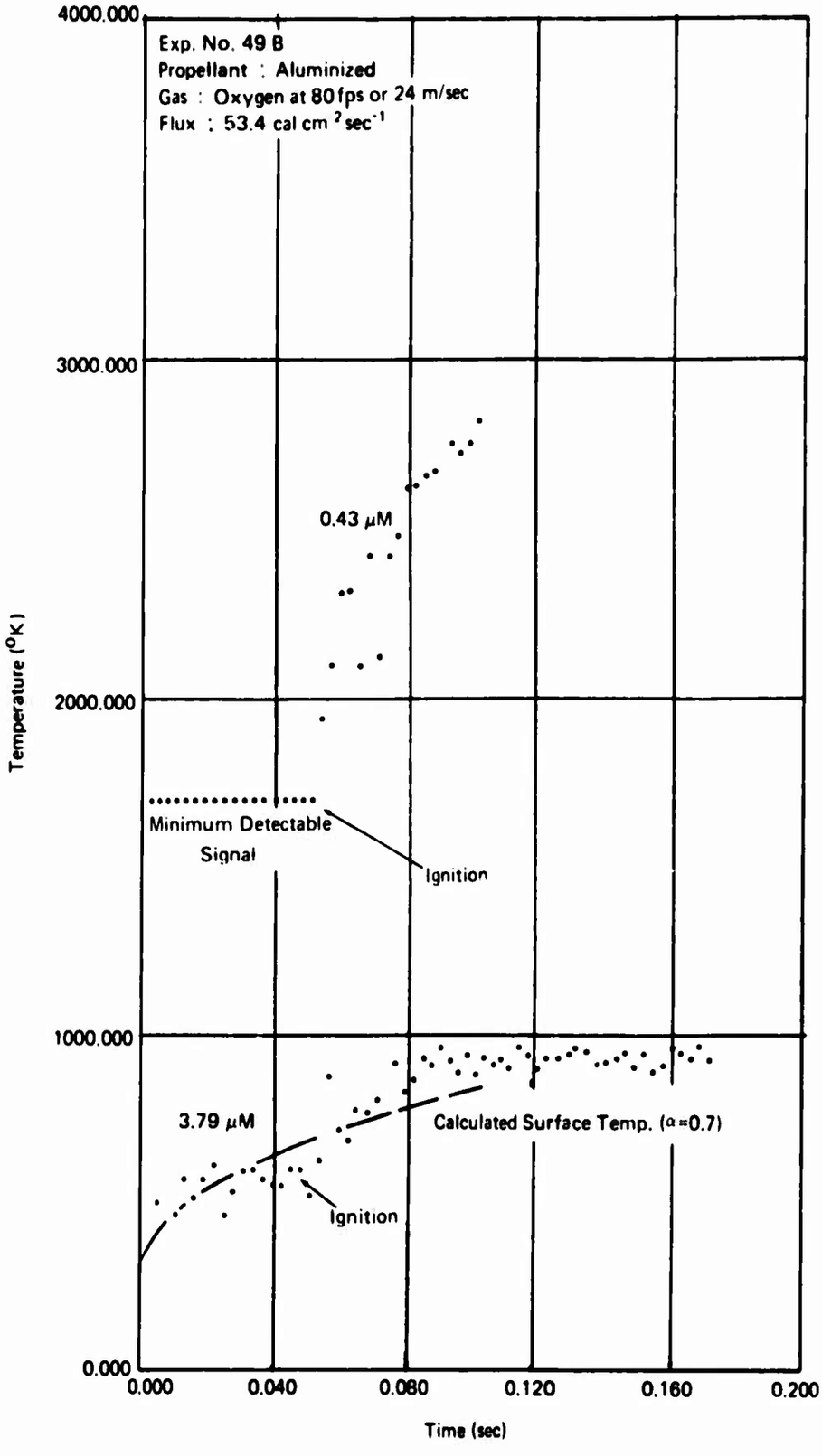

FIGURE 4.2 RADIATIVE IGNITION OF ALUMINIZED PROPELLANT IN AN OXIDIZING ATMOSPHERE

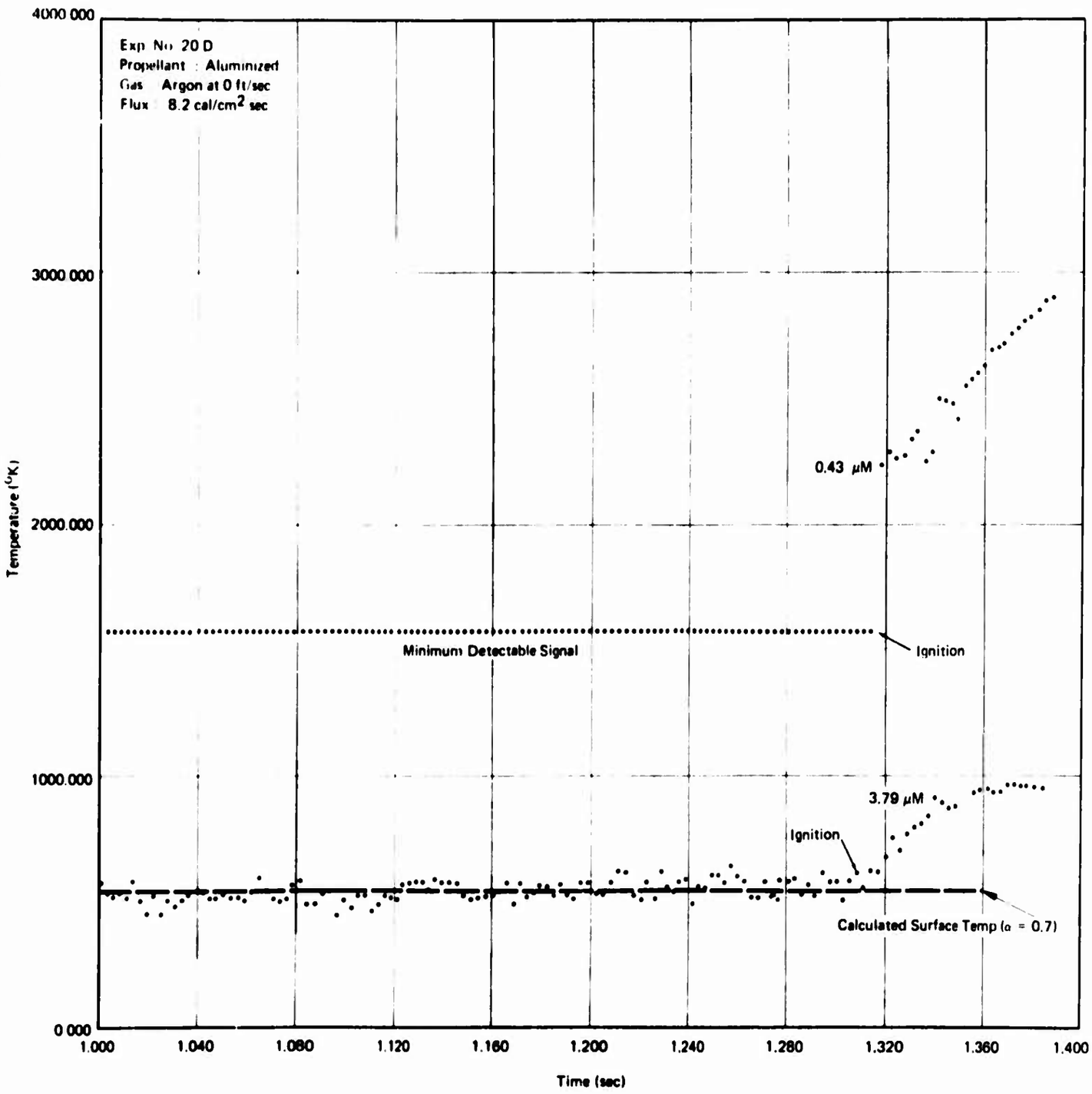

FIGURE 4.3 RADIATIVE IGNITION OF ALUMINIZED PROPELLANT IN AN INERT ATMOSPHERE

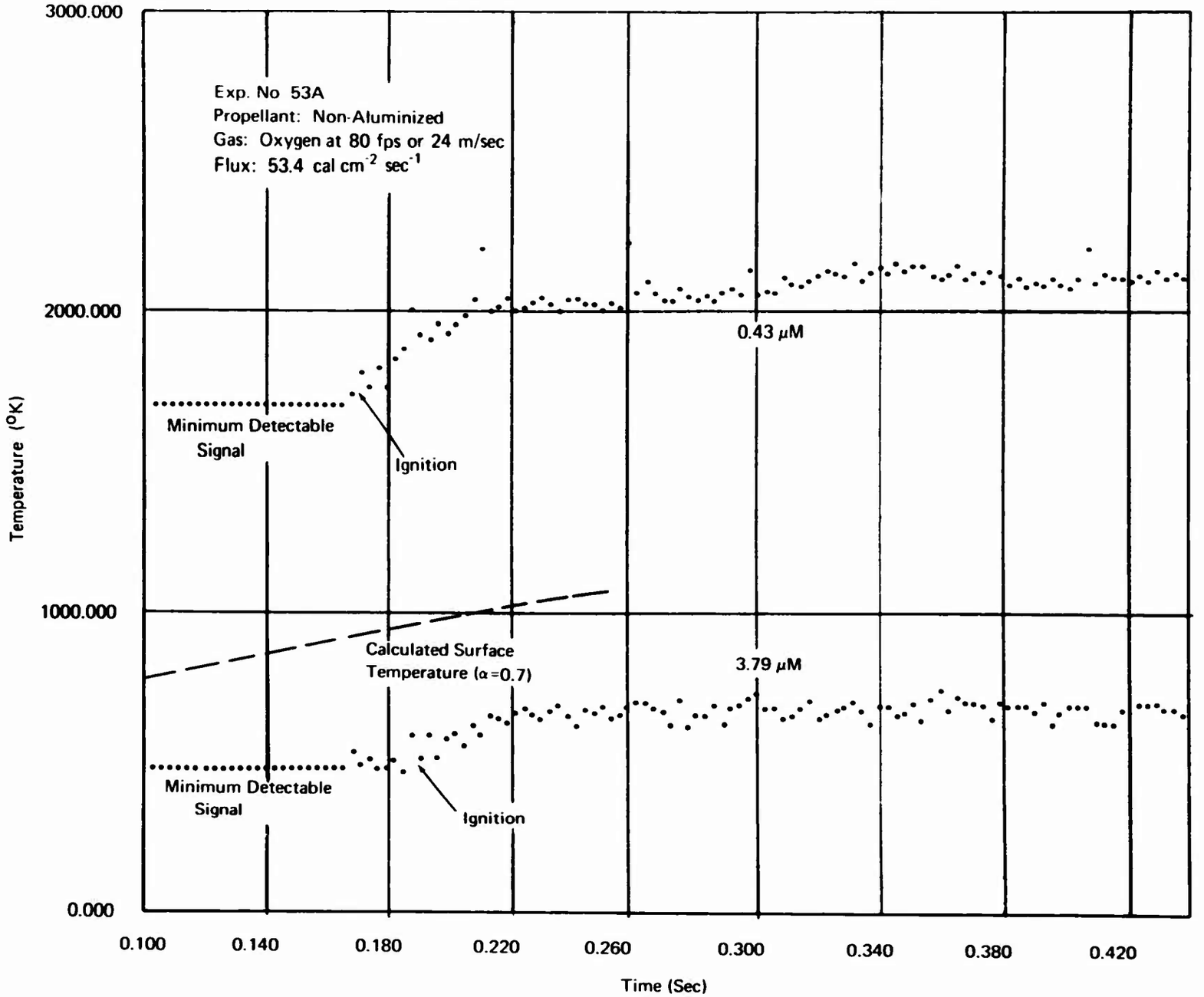

FIGURE 4.4 RADIATIVE IGNITION OF NON-ALUMINIZED PROPELLANT IN AN OXIDIZING ATMOSPHERE

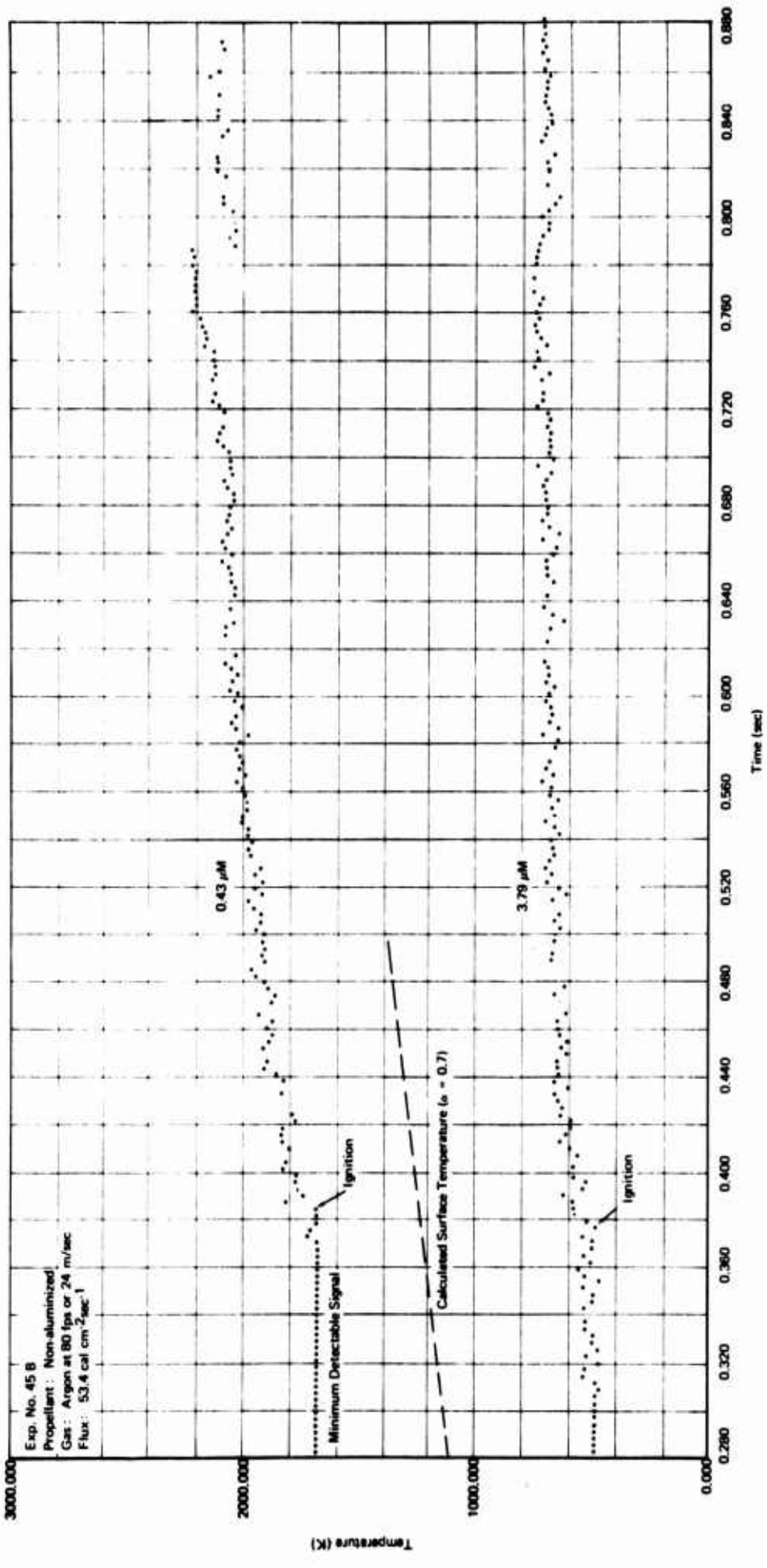

FIGURE 4.5 RADIATIVE IGNITION OF NON-ALUMINIZED PROPELLANT IN AN INERT ATMOSPHERE

TABLE 4.1

Radiative Heating Ignition Delay Data

Experiment Number	Gas	Gas Flow Rate (m/sec)	Heat Flux (cal/cm^2 sec)	Ignition Time (msec) τ_{ir}	Ignition Time (msec) τ_{vis}	Ignition Temperature T_{ig} (°K)	Steady State Temperature T_s (°K)
Non-Aluminized Propellant							
35B	Argon	0	17.5	3392	3401	550	780
35C	Argon	0	17.5	4106	4080	550	760
35D	Argon	0	17.5	3238	3240	560	760
35E	Argon	0	17.5	2237	2240	560	760
47	Argon	0	53.4	1960	1928	540	760
45B	Argon	24	53.4	377	384	510	700
54A	Oxygen	24	35.1	746	740	540	690
53A	Oxygen	24	53.4	186	166	500	690
Aluminized Propellant							
20A	Argon	0	8.2	1482	1486	620	970
20B	Argon	0	8.2	1580	1584	600	960
20C	Argon	0	8.2	1505	1501	600	960
20D	Argon	0	8.2	1308	1316	580	960
31A	Argon	0	8.2	1916	1912	580	970
46	Argon	0	53.4	53	56	590	990
44A	Argon	24	53.4	44	48	560	950
55A	Oxygen	24	35.1	120	144	520	930
49B	Oxygen	24	53.4	51	52	580	940

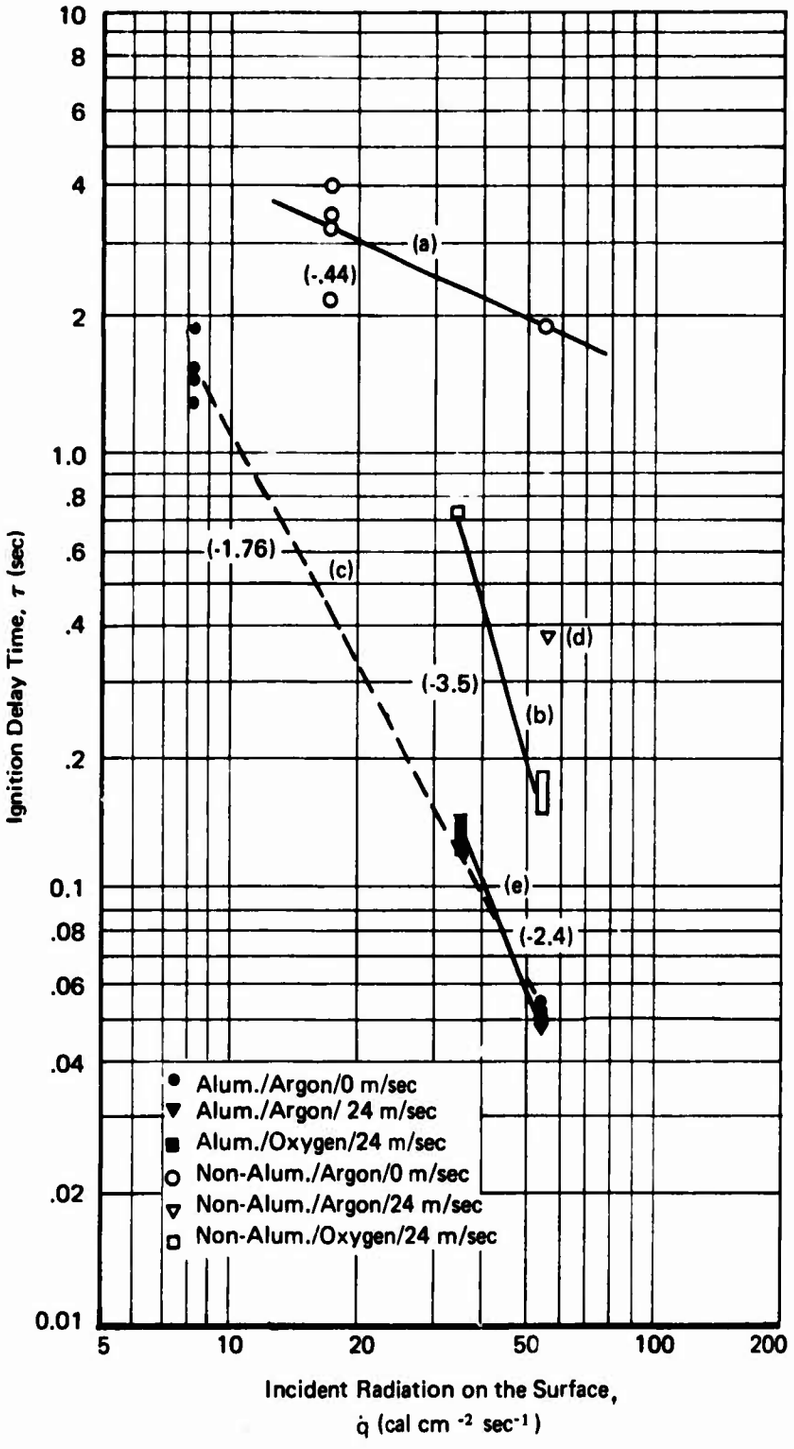

FIGURE 4.6 **ALUMINIZED AND NON-ALUMINIZED PROPELLANT IGNITION BY RADIATIVE HEATING. IGNITION DELAY TIME VERSUS RADIANT FLUX**

and plotted in Figure 4.6.

Ignition temperatures measured at τ_{ir} varied between 520 and 620°K for the aluminized propellant with an average of 578°K and between 500 and 550°K for the non-aluminized propellant with an average of 539°K. After ignition had been established, steady state surface temperatures, T_s, averaged 959°K for the aluminized propellant and 738°K for the non-aluminized propellant. The ignition steady state surface temperatures were generally lower when the surrounding gas was allowed to flow at 24 m/sec.

Although differences in the ignition delay times τ_{vis} and τ_{ir} as measured by the visible and IR radiation detectors were observed, the statistical significance of these differences could not be determined because of the limited number of tests performed. However, the fact that some relatively large differences (24 msec in No. 55A, 20 msec in No. 53A) were observed in some of the runs, warrants a recommendation for the need to investigate this matter further.

For opaque inert solids heated by a constant flux of energy, Equation (2.2) predicts that a plot of τ versus $\dot{q}$ should have a slope of -2. Upon examining the experimental data which are plotted in Figure 4.6, one can make the following observations:

1. Ignition times for the non-aluminized propellant were considerably greater than those for the aluminized propellant at the same incident heat fluxes.

2. For quiescent argon and the non-aluminized propellant, (Figure 4.6 a),

$$\tau \sim \dot{q}^{-.44}$$

3. For oxygen at 24 m/sec and the non-aluminized propellant (Figure 4.6 b)

$$\tau \sim \dot{q}^{-3.5}$$

Argon at 24 m/sec (Figure 4.6 d), produced a greater time delay than

oxygen at the same heat flux and flow rate.

4. For quiescent argon and the aluminized propellant (Figure 4.6 c)

$$\tau \sim \dot{q}^{-1.76}$$

5. For the aluminized propellant, the line for oxygen at 24 m/sec, (Figure 4.6 e), had a slope ($\sim$ -2.4) slightly greater than that for quiescent argon (Figure 4.6c).

The translucency of the non-aluminized propellant and the resulting dissipation of energy incident at the surface by optical absorption within the propellant explains the long delay in ignition and why the predicted heating curves in Figures 4.4 and 4.5 do not coincide with the surface temperature curve measured by the IR detector. This also explains why the plot for the aluminized propellant, (Figure 4.6 c), which is essentially opaque to thermal radiation when surrounded by quiescent argon gives a slope of -1.76 which is nearer to the predicted theoretical slope of -2. The increase in slope of lines (e) and (b) can be attributed to the loss of heat by convection to the moving gas stream[6]. Since Equation (2.2) can be written in the form

$$\tau = \text{const. } k\, \dot{q}^{-2} \qquad (4.1)$$

an effective decrease in $\dot{q}$ (due to convection losses) appears as a decrease in the slope of τ vs. $\dot{q}$.

As ignition times become very long, as is the case in Figure 4.6a, the thermal penetration distance δ_T, becomes greater. This distance is given by[14]

$$\delta_T \simeq 4\sqrt{\alpha\tau} \qquad (4.2)$$

where α = thermal diffusivity

For the propellant employed in this study, α is estimated at 2.94×10^{-3} cm^2/sec. For ignition delays of 1 and 4 seconds, δ_T = .22 cm and .44 cm respectively. These depths are of the same magnitude as the depth of the propellant in the holder (.32 cm) and thus Equation (2.2) which was

derived for a semi-infinite solid is not applicable. The loss of heat to the metal holder can be thought of as a fictitious increase in the thermal conductivity of the propellant. A fictitious increase in k in Equation (4.1) is reflected as an increase in the slope of τ vs. $\dot{q}$. Figure 4.6a gives a slope of -0.44 as opposed to the theoretically predicted slope of -2.

The reduction in ignition delay of the non-aluminized propellant when oxygen was allowed to flow past the propellant surface as opposed to argon can be explained by the need for a minimum concentration of oxidizer in the boundary layer in order to have ignition. For the aluminized propellant, however, regardless of the adjacent gas or its velocity, there were no significant differences in ignition delay. Thus, aluminimum seems to play a significant role in ignition initiation, but this role is not completely understood.

V. PROPELLANT IGNITION BY CONVECTIVE HEATING

5.1 Apparatus

The hot gas tunnel[3] shown in Figure 5.1 was used to study ignition by convective heating. The apparatus employed a mixture of gases which were fed automatically and sequentially into the combustion chamber and ignited. A celluloid diaphragm at the test section orifice opening and helium injected into the test section prevented the hot gases from reaching the propellant while the combustion gases were exhausted through two orifices in the combustion chamber. When the diaphragm was ruptured, a small fraction of the combustion gases was diverted into the test section and exhausted at sonic velocity through the orifice. It had been shown in a previous study[3] that constant heat flux could be obtained in this apparatus with $CO-O_2-N_2$ mixtures.

By changing either the combustion chamber pressure or the diameter of the test section orifice, the pressure level in the test section and thus the gas flow rate and the heat flux level could be altered.

The sample holder was identical to that used in the radiative heating tests (see § 4.1) and the manner of sample preparation was similar.

Another type of sample holder was employed in experiments #114 and 115. The cavity in these tests was elongated as shown in Figure 5.2. The hot gases could thus be made to arrive at the point observed by the optical detector (center of metal plug) after passing over the metal surface, or (by rotating the sample holder 180°) after passing over the propellant.

Pressure in the test section was monitored with a water-cooled strain-gauge transducer. Heat transfer rates were measured with a Nanmac surface thermocouple. It was assumed that the heat transfer rate indicated by the Nanmac gauge which was embedded in a stainless steel block was the same as the initial rate experienced by the propellant sample. This assumption was less valid as the test proceeded because the temperature depended on the thermal properties of the sample and its

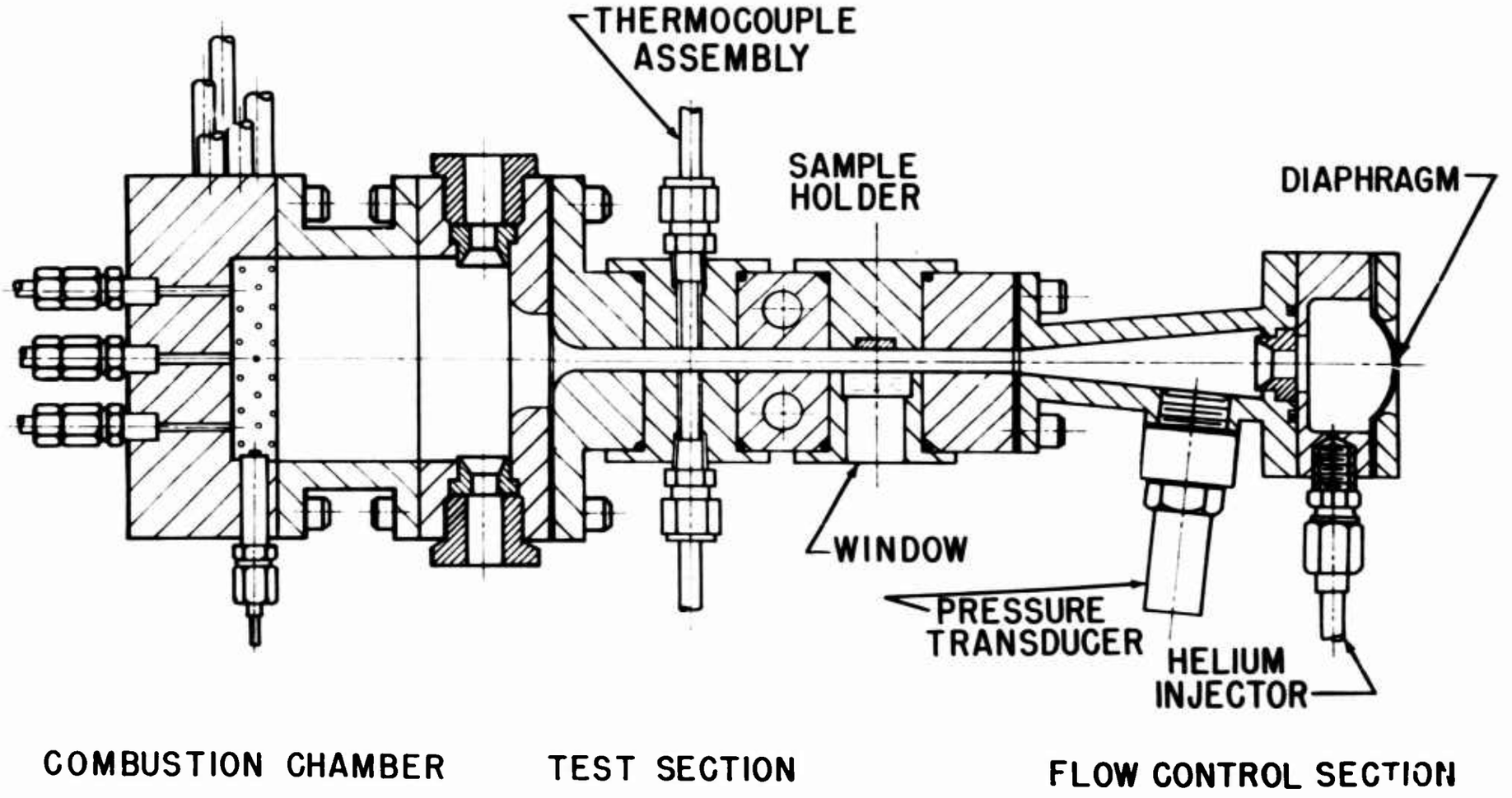

FIGURE 5.1 HOT GAS TUNNEL FOR CONVECTIVE HEATING

FIGURE 5.2 HOT GAS TUNNEL SAMPLE HOLDERS

holder and on whether or not the surface melted, evaporated or ablated.

The optical detector was sighted at the propellant sample through a quartz window. A chopper wheel with 1 msec cycle was used. Outputs of the IR and visible radiation detectors, the pressure transducer and the heat flux meter were recorded on a fast response multichannel recorder. In addition, the rupture of the disc was indicated on the same chart by breaking an electric circuit through a narrow strip of aluminum foil stretched across the diaphragm. A typical recorder output is shown in Figure 5.3.

5.2 Test Conditions

The two propellants used in the radiative heating study were again used here. Three gas mixtures were used in the hot gas tunnel:

$$CO + .345O_2 + .53N_2 \longrightarrow .69\ CO_2 + .31CO + .53N_2$$

$$CO + .875\ O_2 + .5N_2 \longrightarrow CO_2 + .375O_2 + .5N_2$$

$$CO + .975O_2 \longrightarrow CO_2 + .425O_2$$

In all cases, a very small amount of hydrogen (0.2 mole%) was added to the mixture to aid ignition. The fuel rich gas mixture was operated at two pressure levels of $\sim$31 and $\sim$64 psia with corresponding heat fluxes of $\sim$38 and $\sim$54 cal/cm^2 sec. The other two mixtures were oxygen rich and were operated at one pressure level of about 30 psia which gave a corresponding heat flux of about 30 cal/cm^2 sec.

5.3 Presentation of the Results

The outputs of the IR and visible radiation detectors were converted to temperature-time curves for a representative sample of the runs. Typical results for the aluminized propellant are shown in Figures 5.4 and 5.5 and for the non-aluminized propellant in Figures 5.6 and 5.7. Again, two ignition delay times were determined, one from the time of disc rupture to the point where there was a change in the rate of temperature rise in the IR detector output and the other to the point

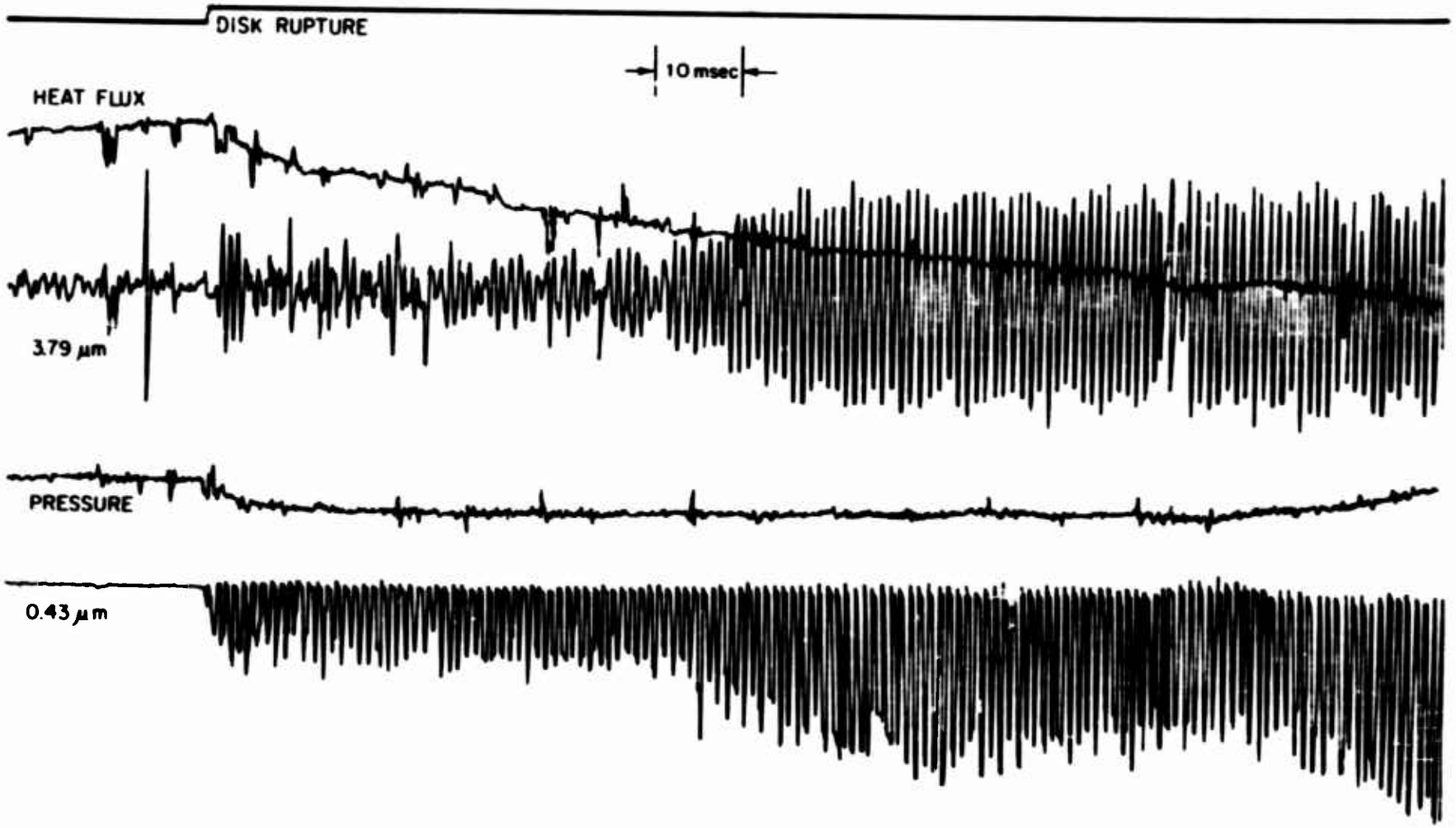

FIGURE 5.3 TYPICAL RECORDER OUTPUT DURING IGNITION

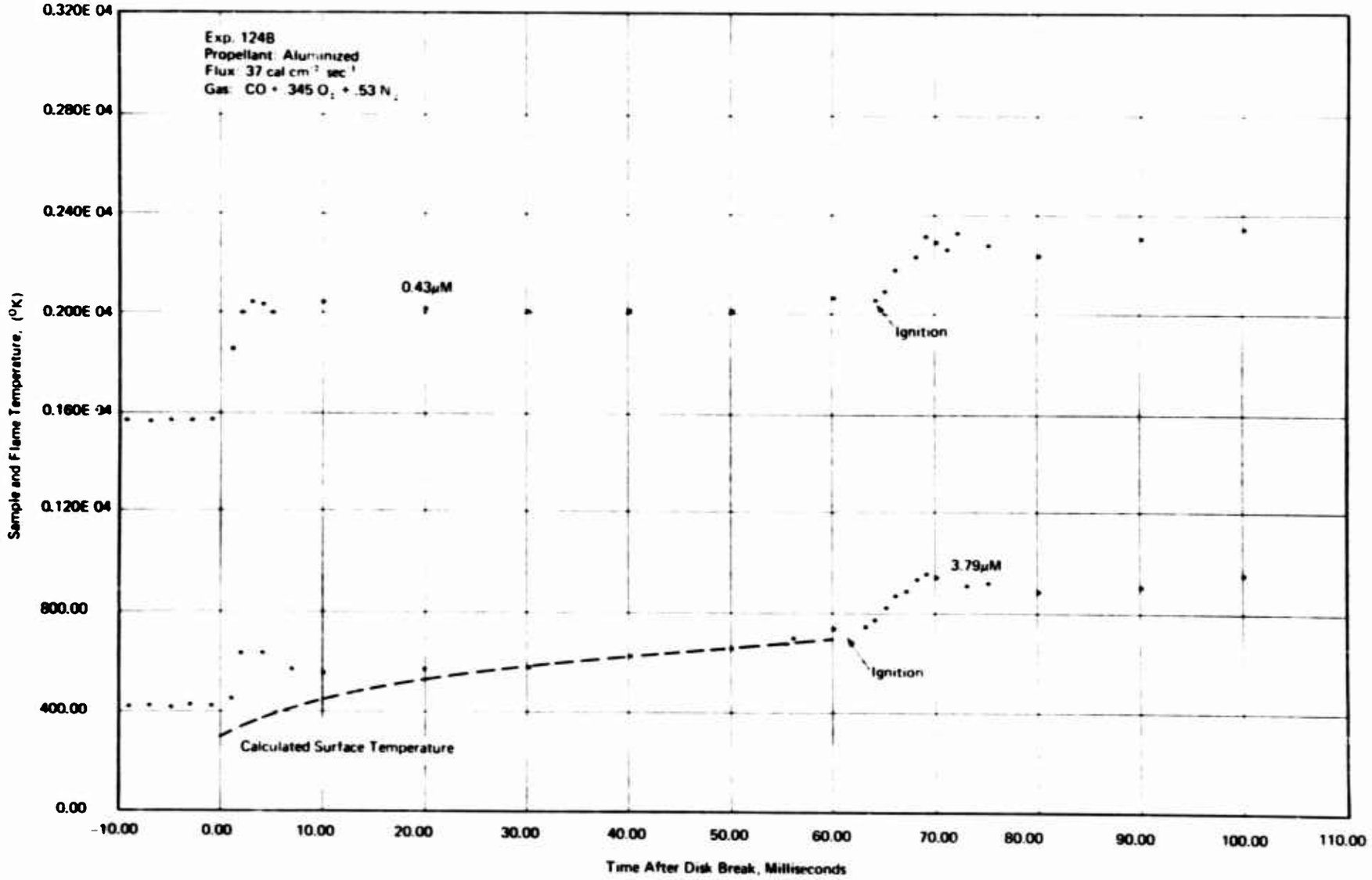

FIGURE 5.4 CONVECTIVE HEATING OF ALUMINIZED PROPELLANT WITH FUEL-RICH GAS

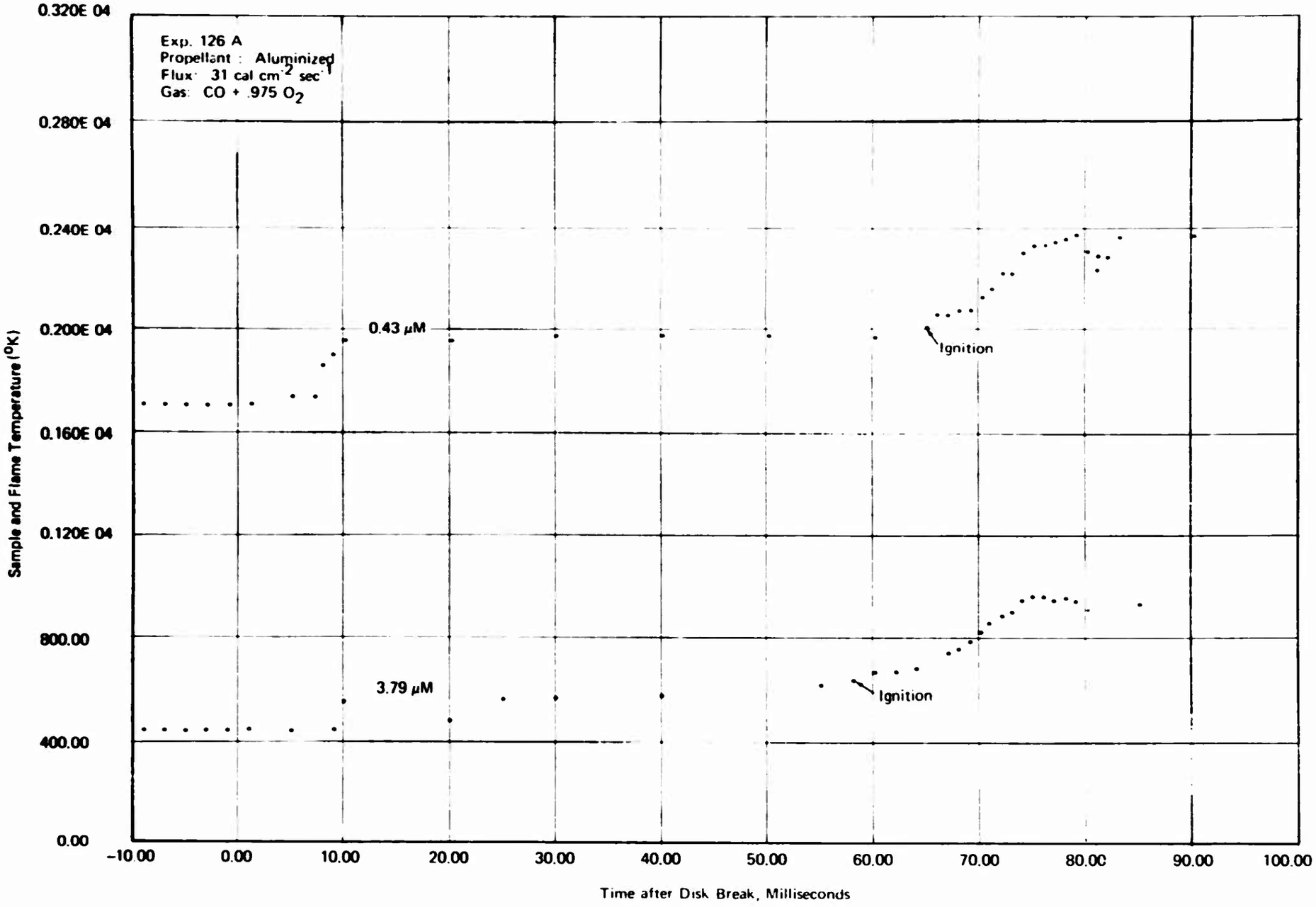

FIGURE 5.5 CONVECTIVE HEATING OF ALUMINIZED PROPELLANT WITH OXYGEN-RICH GAS

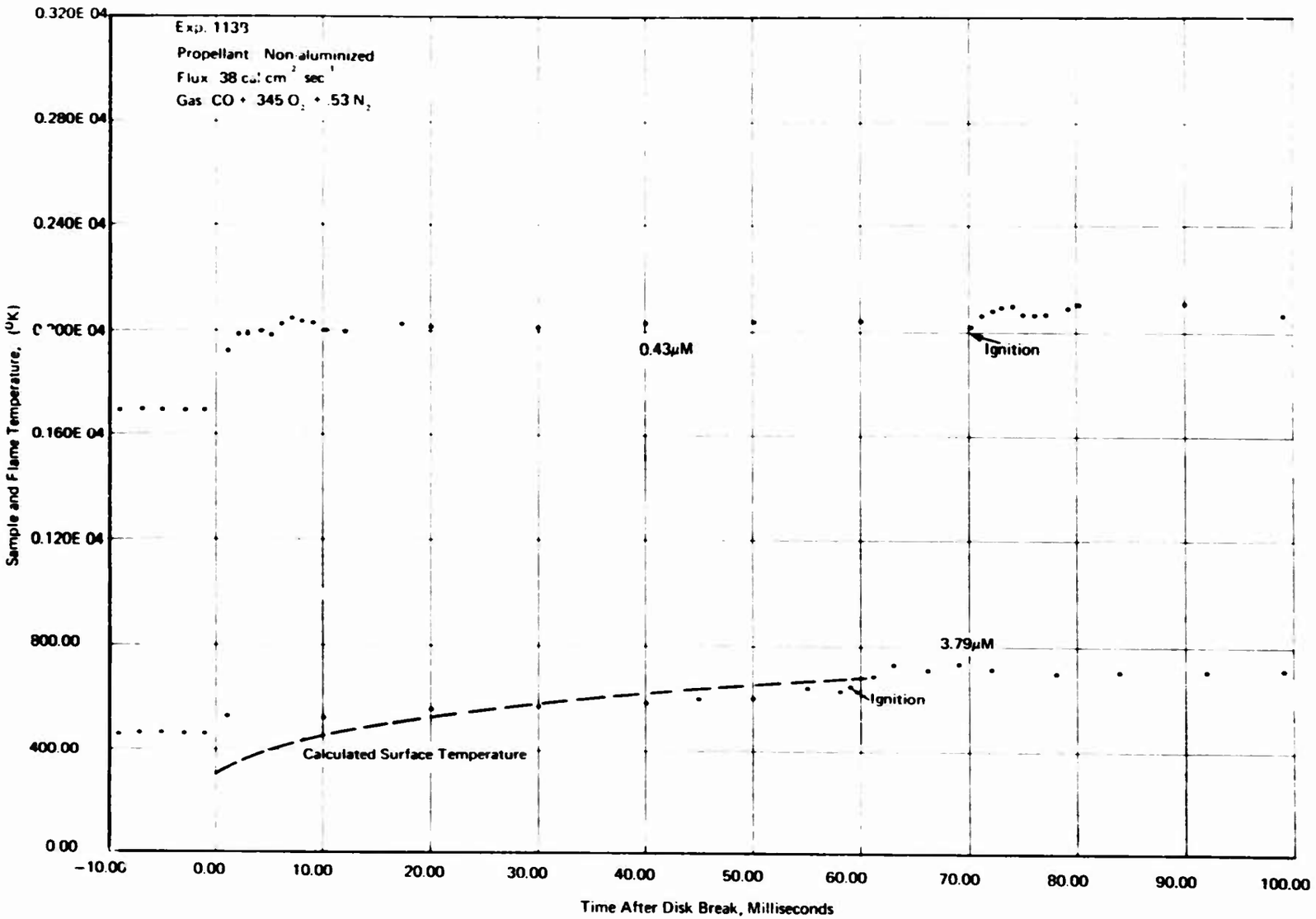

FIGURE 5.6 CONVECTIVE HEATING OF NON-ALUMINIZED PROPELLANT WITH FUEL-RICH GAS

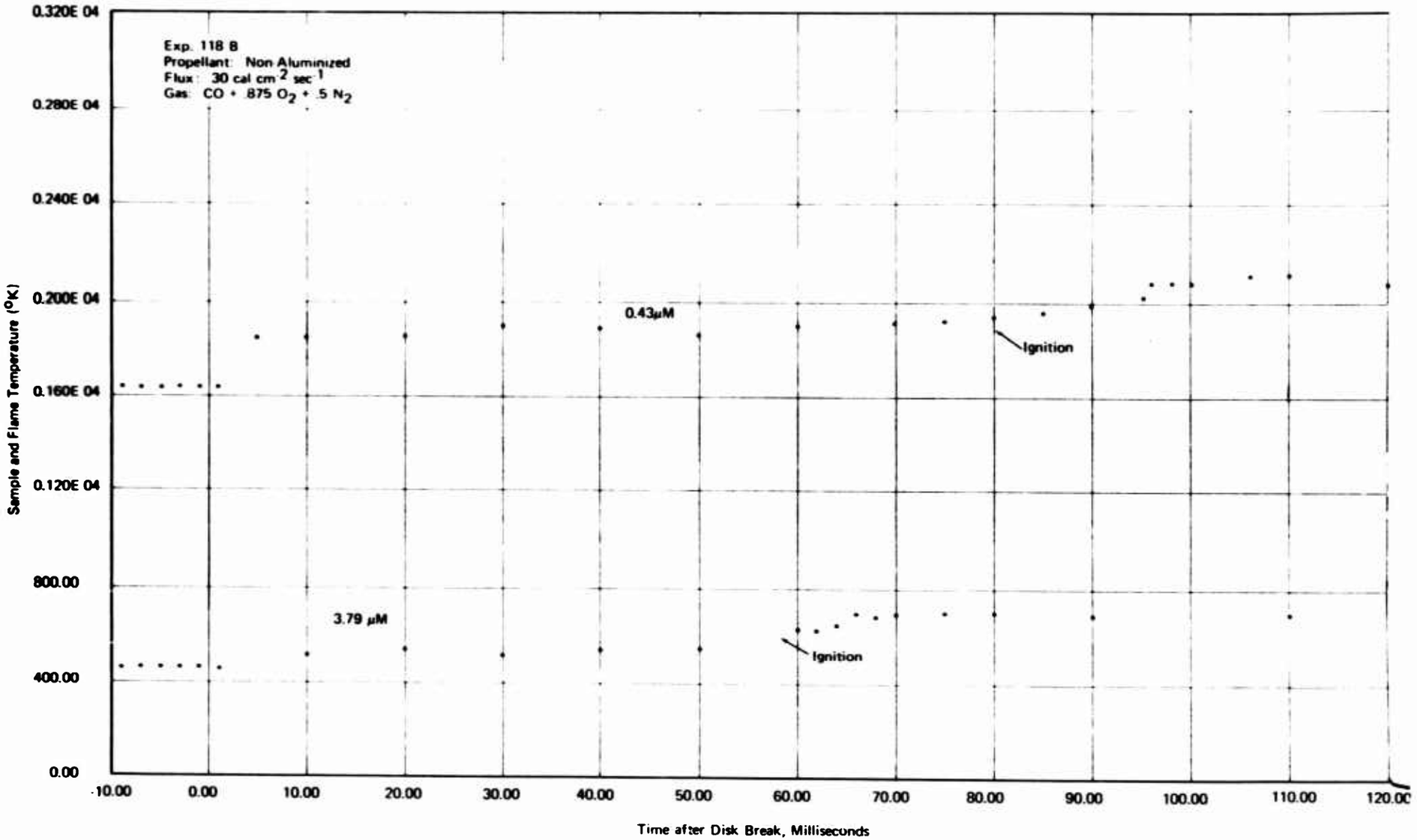

FIGURE 5.7 CONVECTIVE HEATING OF NON-ALUMINIZED PROPELLANT WITH OXYGEN-RICH GAS

where there was an increase in flame temperature as depicted by a rise in the visible radiation detector output. The ignition delay results for convective heating with an oxygen difficient gas mixture at two pressure (and heat flux) levels are given in Table 5.1 and plotted in Figure 5.8. The heat flux was calculated by substituting the Nanmac surface thermocouple data and the physical properties of stainless steel into the general form of Equation (2.2). Since it had already been shown that the apparatus produces a constant heat flux[3], only one temperature-time reading was necessary for the calculation. Table 5.2 gives additional data from tests employing the two other gas mixtures which were oxygen rich.

5.4 Discussion of the Convective Heating Results

Figure 5.8 shows that the ignition delay of the aluminized propellant was greater than that for the non-aluminized propellant. This could be attributed to the greater thermal conductivity of the aluminized propellant which lead to a greater dissipation of incident energy. This behavior was just the opposite of the ignition of the two propellants by radiant heating where dissipation of radiant energy in the translucent, non-aluminized propellant lead to longer delays than in the relatively opaque aluminized propellant (see Figure 4.6).

It was difficult to make more generalizations with the limited amount of data that were obtained. The aluminized propellant data including its slope of -2.5 were in agreement with the data obtained previously by Bastress and Niessen[4]. The aluminized propellant data were also in fair agreement with the radiative heating line for the aluminized propellant surrounded by quiescent argon. The radiative ignition line was transposed from Figure 4.6 after correcting for the absorptivity of the propellant surface by multiplying $\dot{q}$ by 0.7. No data were available for an overall absorptivity. A previous investigation of the variation of absorptivity with wavelength has shown[1] that it varied from 0.8 in the visible region to less than 0.7 at 2 μM.

In all the convective heating runs, ignition was sensed by the IR detector before it was detected by the visible radiation detector. It is

TABLE 5.1

Ignition Delay Data for Convective Heating With Combustion Products of $CO + .345O_2 + .53N_2$

Experiment Number	Chamber Pressure (psia)	Heat Flux (cal/cm^2 sec)	Ignition Time (msec) τ_{ir}	Ignition Time (msec) τ_{vis}	$\Delta\tau$	Ignition Temperature T_{ig} (°K)	Steady State Temperature T_s (°K)
Non-Aluminized Propellant							
113 A	34	38	61	70	9	620	700
B	31	38	59	73	14	650	720
C	33	38	59	72	13		
D	31	41	--	--	--		
E	31	38	56	72	16	620	720
116 A	62	--	--	--	--		
B	65	53	3	14	11		
C	66	58	13	20	7	580	720
D	63	53	--	--	--		
Aluminized Propellant							
124 A	32	37	85	88	3		
B	31	37	62	64	2	720	940
C	31	35	83	88	5		
125 A	62	--	27	30	3		
B	--	54	29	31	2		
C	62	52.5	28	31	3	720	900
Elongated Non-Aluminized Propellant							
114 A	32	--	47	56	9	600	710
B	32	39	50	53	3		
115 A	32	48	52	63	11		
B	32	41	60	(80)*	(20)	600	710

*Ignition point was difficult to identify because of gradual change.

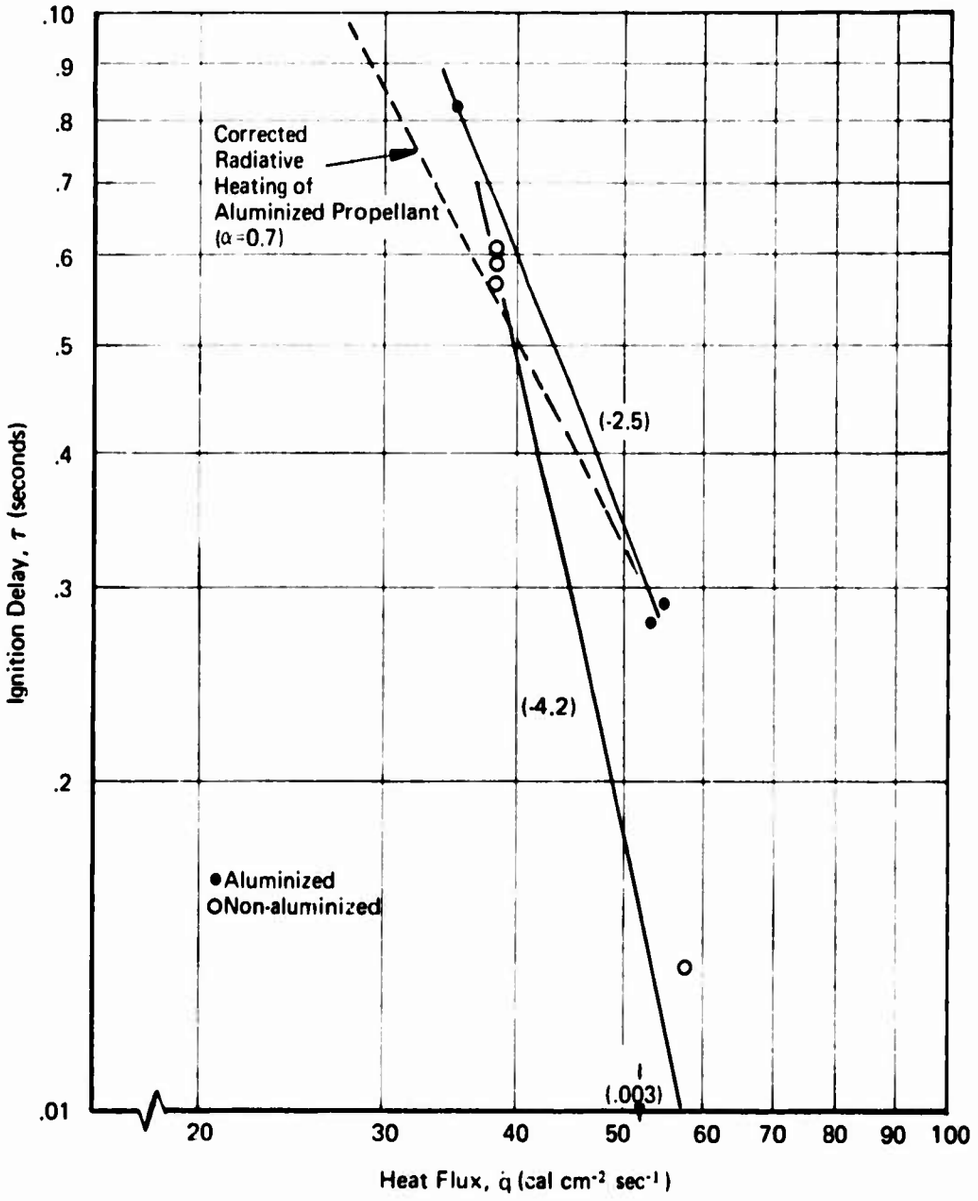

FIGURE 5.8 **IGNITION DELAY OF ALUMINIZED AND NON-ALUMINIZED PROPELLANT UNDER CONVECTIVE HEATING WITH COMBUSTION PRODUCTS OF CO + .345 O_2 + .53 N_2.**

TABLE 5.2

Ignition Delay Data for Convective Heating With Oxygen Rich Gases

Experiment Number	Unburnt Gas Comp. $CO:O_2:N_2$	Oxygen Mole Fraction	Total Pressure (psia)	Heat Flux (cal/cm^2 sec)	Ignition Time (msec) τ_{ir}	τ_{vis}	$\Delta\tau$	Ignition Temperature T_{ig} (°K)	Steady State Temperature T_s (°K)
Non-Aluminized Propellant									
118 A	1:.875:.5	0.2	--	--	75	80	5		
B	1:.875:.5	0.2	26	30	58	85	29	580	700
C	1:.875:.5	0.2	26	30	70	80	10		
119 A	1:.925:.0	0.3	30	30	45	54	9		
B	1:.925:.0	0.3	30	31	26	42	16		
C	1:.925:.0	0.3	31	30	26	34	5	600*	700
Aluminized Propellant									
127 A	1:.875:.5	0.2	33	32	106	108	2	720	920
126 A	1:.925:.0	0.3	32	31	58	64	6	640	900

*This temperature corresponds to the IR reading at 26 msec from disc rupture. In this case, the ignition process was extremely gradual so that it was difficult to identify when it occurred.

to be recalled that the IR detector senses propellant surface temperature changes while the visible radiation detector senses an increase in the CH radical over what was originally present in the combustion gases. Since there was only a small amount of hydrogen in the combustion gases with a corresponding small concentration of the CH radical, the generation of the CH radical in the flame from the reaction of the decomposition products of PBAA could be easily sensed by the detector.

The difference in ignition delay time as measured by the two detectors, $\tau_{ir} - \tau_{vis} = \Delta\tau$, was always greater for the non-aluminized propellant. Apparently, because the ignition of the aluminized propellant occurred at higher temperatures, the gaseous decomposition products in the boundary layer above the surface reached their ignition temperature faster than in the case of the non-aluminized propellant. This occurred regardless of whether or not the surrounding hot gas was oxygen rich or deficient.

5.5 Effect of Oxygen Concentration on Ignition Delay

If it is postulated that the propellant combustion is sustained by a heterogeneous surface reaction between the oxidizer and fuel in the condensed state, and that the rate of this reaction reaches a particular level when ignition occurs[1], the dependence of the rate of this reaction on the concentration of the gaseous reactant can be described by the equation

$$r_{ig} = r_o + A\, P_{O_2} \exp\,(-E/RT_{ig}) \qquad (5.1)$$

or

$$\ln \frac{r_{ig} - r_o}{A} = \text{constant} = \ln P_{O_2} - \frac{E}{RT_{ig}}$$

The slope of a plot of $\ln P_{O_2}$ vs. $\frac{1}{T_{ig}}$ would give the value of $\frac{E}{R}$ for the oxygen-surface reaction.

The ignition delays from Table 5.2 were used to calculate T_{ig} from Equation (2.2). The averaged data for the non-aluminized propellant

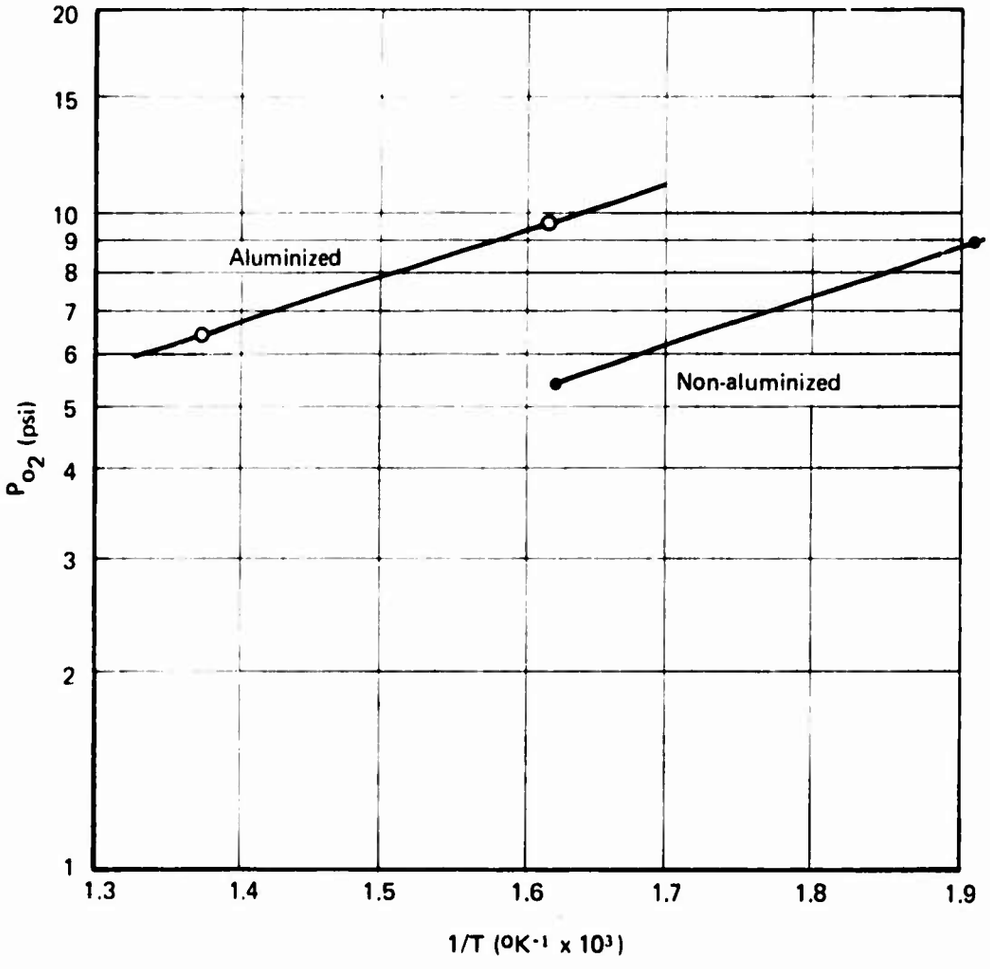

FIGURE 5.9 PLOT OF PARTIAL PRESSURE OF OXYGEN VERSUS RECIPROCAL TEMPERATURE

were used. P_{O_2} was plotted versus $\frac{1}{T_{ig}}$ (Figure 5.9) and the slope used to arrive at the activation energy. The aluminized propellant gave an activation energy of 3.0 kcal/g-mole while the non-aluminized propellant gave a value of 3.54 kcal/g-mole.

5.6 The Results of the Elongated Samples

Examination of Table 5.1 shows that ignition was observed earlier when the hot gas travelled along the propellant surface first rather than the metal surface which meant that ignition started downstream from the propellant leading edge. This had been observed previously by Bastress and Niessen[4] and more recently by Summerfield, et al[15]. This observation is consistent with both a gas-phase ignition mechanism where a certain flammable mixture concentration is necessary in the boundary layer to initiate a reaction as well as with a heterogeneous reaction mechanism where a critical oxidizer concentration is necessary to react with the solid propellant surface.

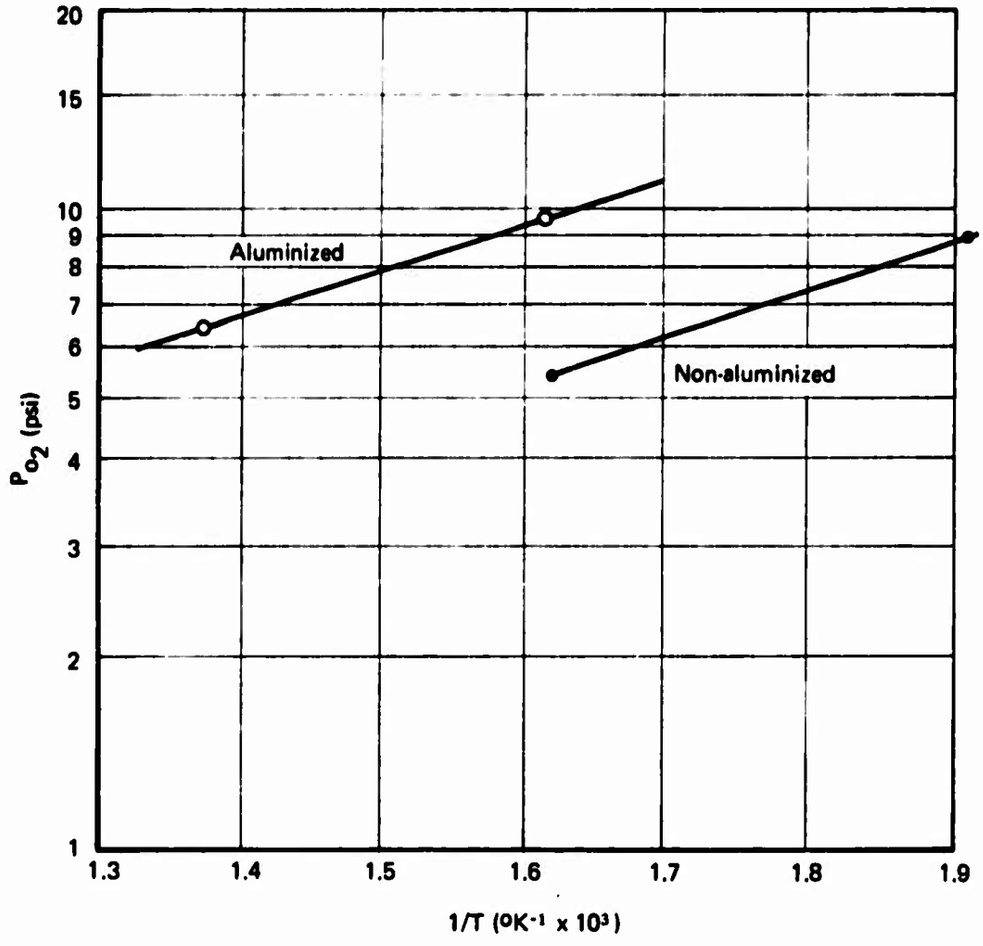

FIGURE 5.9 PLOT OF PARTIAL PRESSURE OF OXYGEN VERSUS RECIPROCAL TEMPERATURE

were used. P_{O_2} was plotted versus $\frac{1}{T_{ig}}$ (Figure 5.9) and the slope used to arrive at the activation energy. The aluminized propellant gave an activation energy of 3.0 kcal/g-mole while the non-aluminized propellant gave a value of 3.54 kcal/g-mole.

5.6 The Results of the Elongated Samples

Examination of Table 5.1 shows that ignition was observed earlier when the hot gas travelled along the propellant surface first rather than the metal surface which meant that ignition started downstream from the propellant leading edge. This had been observed previously by Bastress and Niessen[4] and more recently by Summerfield, et al[15]. This observation is consistent with both a gas-phase ignition mechanism where a certain flammable mixture concentration is necessary in the boundary layer to initiate a reaction as well as with a heterogeneous reaction mechanism where a critical oxidizer concentration is necessary to react with the solid propellant surface.

VI. IGNITION BY CHEMICAL HEATING

It was desired to utilize the detection system described in Chapter III to study ignition under chemical heating conditions. Fluorine gas was chosen as the heating agent mainly because of our familiarity with it in other unrelated studies and because it had been shown to be sufficiently reactive to cause spontaneous ignition without the need for raising the propellant or gas temperature.

6.1 Apparatus

Because of the toxic and fire hazards of fluorine, a great amount of effort was devoted to the design of the system, choice of materials of construction, assembly of the apparatus, and conduct of experiments.

Figure 6.1 is a schematic diagram of the test apparatus. To insure maximum safety for the operating personnel, the entire fluorine section was mounted within a steel cabinet and placed outside the laboratory (Figure 6.2). The fluorine gas pressure gage was visible to the operator through a double window arrangement and the valve stems were extended so that the experiment could be performed and controlled from inside the laboratory. As an added safety feature, the steel enclosure was placed under a slight negative pressure by a fan. A charcoal reactor was used to dispose of the vented fluorine and another to protect the vacuum pump from the small amount of fluorine left in the apparatus after purging. To detect fluorine leaks, a filter paper soaked in potassium iodide was hung in the steel cabinet and was visible through the observation window. The major parts of the apparatus consisted of the fluorine and helium supply bottles, the fluorine disposal reactors, a vacuum pump and the test section. The test section as well as the connecting tubes and valves were made of Monel with Teflon packing. All parts were thoroughly cleaned with acetone then rinsed with a Freon solvent before assembly. The whole apparatus was evacuated and checked for leaks and then pacified with fluorine at 5 psig. A detailed sketch of the test section is shown in Figure 6.3. A rupture diaphragm consisting of a lead-aluminum-lead sandwich was inserted into the flange separating the high-pressure section

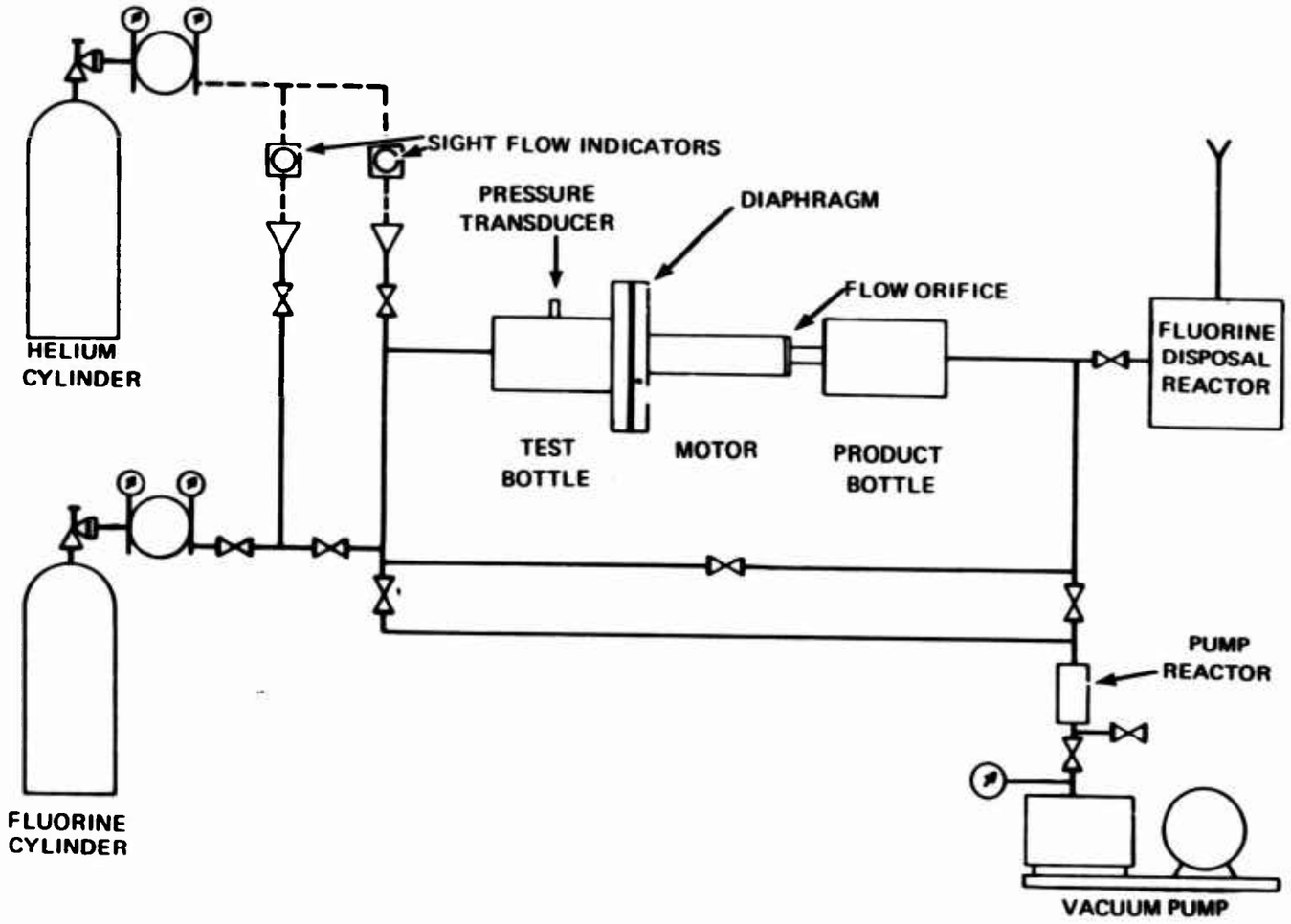

FIGURE 6.1 SCHEMATIC FLUORINE IGNITION TEST APPARATUS

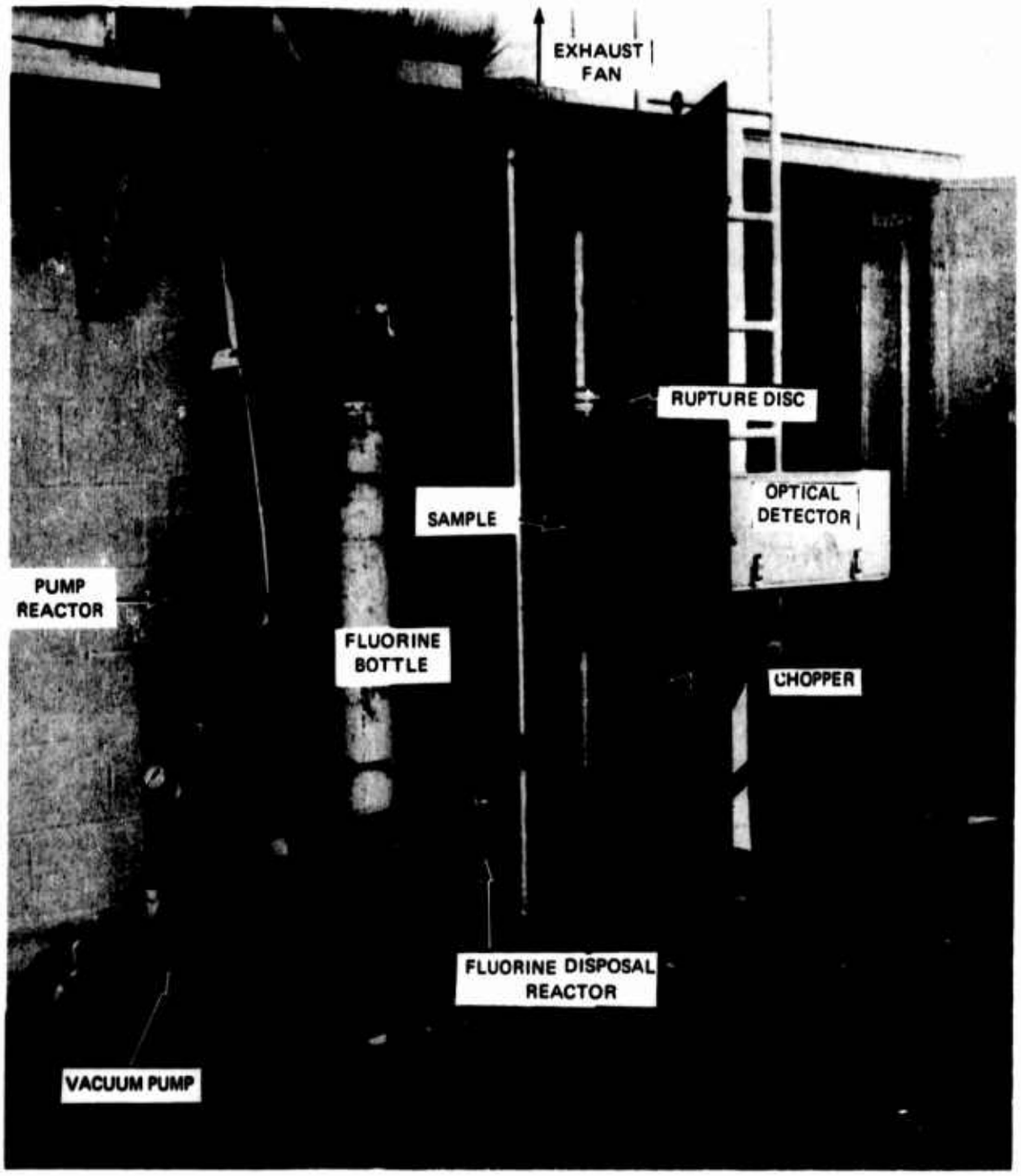

FIGURE 6.2 PHOTOGRAPH OF THE FLUORINE TEST APPARATUS

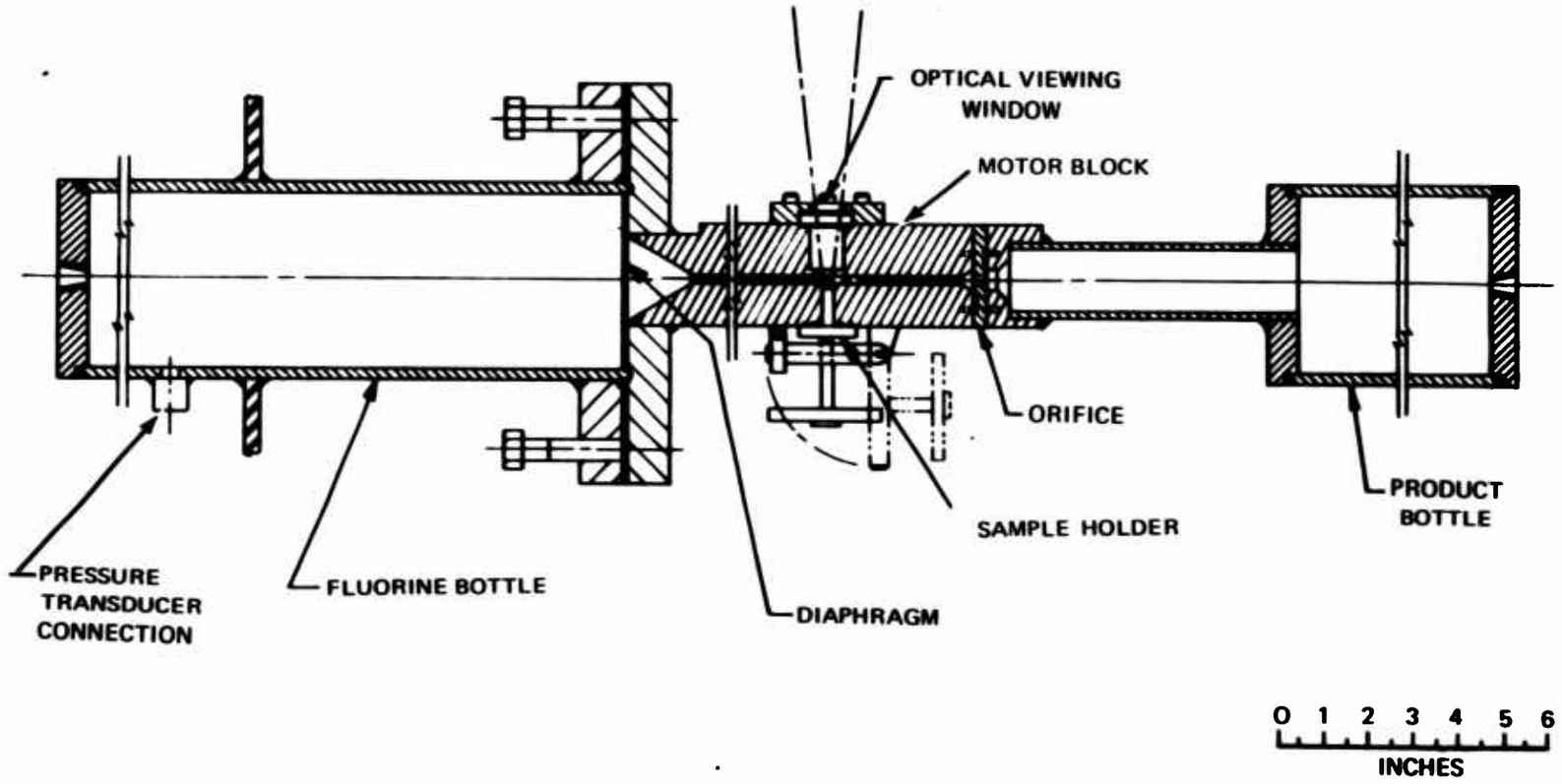

FIGURE 6.3 FLUORINE IGNITION TEST SECTION

of the apparatus from the vacuum section containing the propellant sample. The lead served as a gasket while aluminum served as the rupture disc. The aluminum was an "O" temper 1100 aluminum foil which ruptured at about 32 psia when its thickness was .002 inch and at about 65 psia for a thickness of .003 inch. A good seal was obtained in the flange by preforming the sandwich assembly in a die followed by controlled compression regulated by the use of a predetermined thickness of shim stock between the flanges.

The sample holder was locked into position and sealed to the motor block by a double Teflon O-ring as was the orifice plate. The locking device on the sample holder was designed so that the sample could be easily replaced. Figure 6.4 is a photograph of a ruptured disc and a sample holder.

A pressure strain-gage transducer was used to detect the pressure in the high-pressure section and to determine the point of disc rupture. The optical detector system was mounted outside the steel cabinet and sighted through a sapphire window at the sample. The optical system was covered for protection from the weather and from extraneous sunlight.

6.2 Procedure

The apparatus was purged with helium and vented to the atmosphere through the disposal reactor. A new diaphragm assembly and propellant sample were then inserted into the test section. The system was isolated from the atmosphere and evacuated. The chopper wheel which gave 1 msec cycles was turned on and the instruments activated. Fluorine was introduced into the pressure side of the test section slowly. As the pressure approached the disc-rupture point, the fast response recorder was activated and the pressure raised quickly. After disc rupture, the pressure equalized on both sides of the disc. The flow of fluorine (or fluorine-helium mixture) past the sample was controlled by the orifice size through which flow was sonic for most of the combustion duration and definitely during the initial short ignition period. When the test was completed, the fluorine in the apparatus was vented to the atmosphere through the charcoal bed reactor and purged with helium. The apparatus was then disassembled and the ruptured disc and the sample holder removed.

FIGURE 6.4 PHOTOGRAPH OF A RUPTURED DISC AND A SAMPLE HOLDER

6.3 Test Conditions

A very small amount of the non-aluminized propellant was used in these tests to reduce the probability of a metallic fire. Initially the sample hole in the holder was 1/8 inch in diameter and 1/8-inch deep. No epoxy glue was used in these tests. The propellant was simply pressed into the hole and sliced with a razor so that its surface was flush with the channel wall. The flow-channel cross-section was 1/8 inch x 1/4 inch, and the orifice diameter was 0.143 inch which resulted in a linear gas velocity of $\sim$ 300 ft/sec past the sample (Mach No $\simeq$ .31). All the tests were performed at room temperature ($\sim$ 70°F).

No ignition could be achieved in our initial tests. The sample was allowed to sit in the fluorine atmosphere for more than five minutes with no visible changes in its surface. That the apparatus was working properly was checked by replacing the propellant sample with a tissue paper-rubber cement mixture which was pressed into the sample hole and allowed to dry and cut with a razor flush with the surface. This mixture ignited readily after disc rupture with fluorine. This indicated that the rate of surface heat generation by fluorine reacting with the propellant could not keep up with heat losses by conduction to the surrounding metal and gas and through the propellant. The thermal diffusivity of the propellant is estimated at .003 cm^2/sec while that of paper is about half of that value.

The sample hole was enlarged to 3/16 inch; but again, no ignition could be achieved with a smooth propellant surface. However, when the propellant was allowed to project above the face of the holder and the surface cut (diced) vertically with a razor blade to provide a large area of contact, ignition occurred readily.

6.4 Experimental Results

Two successful runs were made at two different rupture pressures. The first was conducted with a .002-inch rupture disc with pure fluorine. Rupture occurred at 30.3 psia. Ignition delay was about 1 msec as measured by the visible radiation detector and about 2 msec by the IR detector. The second run was made with a .003-inch rupture disc and a mixture

of fluorine and helium. The high-pressure side of the test section was filled with fluorine to 47 psig and then boosted to 52 psig with helium at which pressure rupture occurred. In this case, both the IR and visible radiation detectors indicated that ignition occurred practically instantaneously after disc rupture.

6.5 Discussion of Results

It was observed in both runs that heating of the surface as indicated by the IR detector was more gradual than the signal received from the visible radiation detector which gave a sudden rise almost immediately after rupture. The visible radiation signal diminished quickly to a relatively constant level. This behavior could be attributed to the large exposed surface area containing a large amount of loose propellant which probably ignited immediately at first contact with fluorine giving rise to a large amount of combustion products and, consequently, a larger radiation path length and greater signal. When the heat penetrated to the solid surface, an IR signal was received.

With the limited amount of data that could be obtained, only qualitative observations can be made. The fluorine concentration in the two runs were 3.18×10^{-3} gm/cc and 6.5×10^{-3} gm/cc, respectively. The data of Anderson, et al[16] on the hypergolic ignition of PBAA/AN propellant with an unidentified oxidizer were correlated by Price, et al[6]. A plot of ignition delay vs. oxidizer concentration in gm/cc gave a slope of -2 indicating a first-order reaction as predicted by Equation (2.6). The line was also consistent with a zero activation energy.

For oxidizer concentrations equivalent to those employed in this study, Andersons' data predict 3 and .8 msec ignition delays. These values are close to those obtained in this study considering that errors in our estimates of ignition delay are of the order of $\pm$ 1 msec.

Although this study has shown that the optical detection system could be applied to detect ignition by chemical heating, more work is needed to perfect the ignition system and the instrumentation. A better detection method for the disc rupture should be devised. Furthermore,

it would be desirable to use a recorder capable of detecting time delays of the order of 0.1 msec in these tests because of the short ignition delays encountered. The possibility of using larger flat samples to achieve ignition without having to pile the propellant above the surface should be investigated. This could not have been done initially without being assured of the safety of the procedure.

VII. GENERAL CONCLUSIONS AND COMMENTS

In their classic review of propellant ignition theories, Price et al[6] enumerated the several combinations of reactants and the wide variety of reactions that could take place during the ignition process of a composite solid propellant. It has been shown experimentally that the environment and the method of heating play an important role in influencing ignition delay and in determining the controlling mechanism for propellant ignition. It is very likely that more than one of the ignition theories enumerated in Section 2.3 are applicable at any one time although one ignition mechanism might be predominating over the others. The oxidizing component of a hot gas environment, for instance, will compete with the oxidizer products of the propellant in reacting with the gaseous products of decomposition and/or the solid surface of the binder. What fraction of ignition is taking place as a heterogeneous reaction or as a gas phase reaction depends on several factors such as the temperatures involved, the diffusion coefficients of the reactants, the flow rate of the environment (boundary layer thickness), the oxidizer concentration, the total pressure, the rate constants and activation energies of the competing reactions, etc.

Thus, even with the added information on the effects of the many variables on ignition delay which were studied in this program, it is not possible to develop and substantiate an adequate unified theory that will tie all observed events together.

The results of this investigation do show some trends, however, that are worth noting. These are as follows:

1. The values of T_{ig} were found to be higher when both propellants were ignited by convection as contrasted to ignition by radiation. One explanation could be that due to the higher gas velocity in the convective experiments the concentration of reactive species in the boundary layer is reduced. In order to produce the concentrations necessary for ignition to occur,

the propellant surface temperature must be raised so that they are produced at a faster rate. Ignition delay τ_{ir} was shorter than τ_{vis} when the propellant was ignited convectively. Although the minimum measurable temperature that could be detected in propellant heating may have been too high for this effect to be observed during radiative heating, the available data indicated that the difference between τ_{ir} and τ_{vis} was negligible when the propellants were ignited by radiation. An explanation of this phenomenon might be that again because of the higher flow velocities during convective heating, there had to be a higher rate of generation of reactive species which in this case may have been aided by chemical heat generation on the surface of the propellant, giving rise to an earlier rise in the IR signal.

2. The presence of excess oxygen in the convective heating medium and in the atmosphere surrounding the propellant during radiative heating produced shorter ignition delays. This indicates that the concentration of oxygen in the boundary layer can be important to the ignition process.

3. When the propellant sample was elongated, ignition took place sooner when there was propellant surface upstream of the point at which ignition was detected. This might be attributed to the growth of the boundary layer containing reactive species with distance downstream from the leading edge.

Although these trends are qualitative and are based on limited information, they do suggest, at least, that the ignition of composite propellants may be governed by the requirement that the concentration of the oxidizing species in the boundary layer must reach some critical value.

These observations suggest that further research is needed in the following areas:

1. The establishment of the effect of O_2 concentration and other reactive species in the boundary layer on ignition delay.
2. The need for more experimental data in order to establish statistical significance of results.
3. Further theoretical studies to develop an ignition model using these results.

It is evident from the results of this program that without an adequate model of the ignition process, the data derived from one mode of testing is difficult to extrapolate to another. This implies that radiative testing, for instance, should be used to evaluate the performance of propellants which are normally ignited by igniters that function primarily by radiative heating. The same applies to convective and chemical heating.

This study has also shown that ignition delay is not only affected by environmental factors such as heat flux, mode of heating, gas flow rate, oxidant concentration, etc., but that it was also dependent on the system used for detection. It is therefore recommended that standard igniter tests and the methods used to detect ignition be reexamined.

This study has shown that chemical heating could provide very short ignition delays. Since this can be important in a practical sense for some solid propellant motors, it is recommended that more effort be devoted to the evaluation of this technique. In particular, more data are needed to relate ignition time to total pressure, oxidizer concentration and flow rates, and propellant surface characteristics.

VIII. REFERENCES

1. E. K. Bastress, D. S. Allan and D. L. Richardson, "Solid Propellant Ignition Studies", Technical Documentary Report No. RPL-TDR-64-65, Contract AF04(611)-9065, (October 1964).

2. W. R. Niessen and E. K. Bastress, "Solid Propellant Ignition Studies", Technical Report No. AFRPL-TR-66-32, Contract AF04(611)-10741, (February 1966).

3. E. K. Bastress and W. R. Niessen, "A Hot-Gas Tunnel for Convective Heating Experiments", Journal of Spacecraft and Rockets, 5 (2), 211-213, (1968).

4. E. K. Bastress and W. R. Niessen, "Solid Propellant Ignition by Convective Heating", Final Report No. AFOSR67-0932, Contract AF49(638)-1120, (October 1966).

5. D. S. Allan, E. K. Bastress and K. A. Smith, "Heat Transfer Processes during Ignition of Solid Propellant Rockets", Journal of Spacecraft and Rockets, 4(1), 95-100, (1967).

6. E. W. Price, H. H. Bradley, Jr., G. L. Dehority and M. M. Ibiricu, "Theory of Ignition of Solid Propellants", AIAA Journal, 4 (7), 1153-1181 (1966).

7. R. S. Brown, R. Anderson and L. J. Shannon, "Ignition and Combustion of Solid Rocket Propellants", in Advances in Chemical Engineering, Vol. 7, T. B. Drew et al editors, Academic Press, New York (1968), pp. 1-69.

8. J. H. Frazer and B. L. Hicks, "Thermal Theory of Ignition of Solid Propellants", Journal Phys. Colloid Chem., 54, 872-876 (1950).

9. H. S. Carslaw and S. L. Jaeger, Conduction of Heat in Solids , 2nd edition, Clarendon Press, Oxford (1959), p. 75.

10. A. D. Baer and N. W. Ryan, "Ignition of Composite Propellants by Low Radiant Fluxes", AIAA Journal, 3 (5), 844-889 (1965).

11. R. F. McAlevy II, P. L. Cowan and M. Summerfield, "The Mechanism of Ignition of Composite Solid Propellants by Hot Gases", in Progress in Astronautics and Rocketry, Vol. I: Solid Propellant Rocket Research, M. Summerfield, editor, Academic Press, New York (1960).

12. R. B. Beyer, R. Anderson, R. D. MacLaren and W. J. Corcoran, "Ignition of Solid Propellant Motors under Vacuum", Final Report, UTC-2079-FR, Contract AF 04(611)-9701, United Technology Center, Sunnyvale, California (1965).

13. R. Anderson, R. S. Brown, G. T. Thompson and R. W. Ebeling, "Theory of Hypergolic Ignition of Solid Propellants", AIAA Preprint 63-514 presented at AIAA Hetergeneous Combustion Conference, Palm Beach, Florida (1963).

14. R. B. Bird, W. E. Stewart and E. N. Lightfoot, Transport Phenomena 2nd printing, John Wiley and Sons, Inc., New York (1962), p. 354.

15. M. Summerfield, P. L. Stang, C. H. Waldeman, T. Kashiwagi, T. J. Ohlemiller, B. W. MacDonald and R. B. Rothman, "Ignition Mechanisms of Solid Propellants", paper presented at the 5th AFOSR combined Contractors' Meeting on Combustion Dynamics, Denver, Colorado, June 1969.

16. R. Anderson, R. S. Brown, R. Ebeling and R. W. Hawke, "Fundamental Investigation of Hypergolic Ignition for Solid Propellants", (U), United Technology Center, Sunnyvale, California, Report UTC 2018-FR Contract NOw 62-1006-C, (December 15, 1963), Confidential.

Security Classification

DOCUMENT CONTROL DATA - R & D

(Security classification of title, body of abstract and indexing annotation must be entered when the overall report is classified)

1 ORIGINATING ACTIVITY *(Corporate author)* Arthur D. Little, Inc. 20 Acorn Park Cambridge, Massachusetts 02140	2a. REPORT SECURITY CLASSIFICATION UNCLASSIFIED 2b. GROUP

3 REPORT TITLE

THE IGNITION OF SOLID PROPELLANTS BY RADIATIVE, CONVECTIVE AND CHEMICAL HEATING

4 DESCRIPTIVE NOTES *(Type of report and inclusive dates)*

Scientific Final

5 AUTHOR(S) *(First name, middle initial, last name)*

Sami Atallah Donald S Allan Daniel F Comstock Jr and B Bakerjian

6 REPORT DATE November 1969	7a. TOTAL NO. OF PAGES 68	7b. NO. OF REFS 16
8a. CONTRACT OR GRANT NO. F44620-67-C-0002 b. PROJECT NO 9711-01 c. 61102F d. 681308	9a. ORIGINATOR'S REPORT NUMBER(S) [redacted] 9b. OTHER REPORT NO(S) *(Any other numbers that may be assigned this report)* AFOSR 69-3091TR	

10 DISTRIBUTION STATEMENT

1. This document has been approved for public release and sale, its distribution is unlimited.

11. SUPPLEMENTARY NOTES TECH, OTHER	12. SPONSORING MILITARY ACTIVITY Air Force Office of Scientific Research(SREP) 1400 Wilson Boulevard Arlington, Virginia 22209

13 ABSTRACT

This report presents the results of an experimental study in which aluminized and non-aluminized composite solid propellants were ignited under different environmental conditions. Ignition was achieved by radiative, convective and chemical heating. An optical system operating in two narrow wavelength bands was used to detect the onset of ignition on and near the surface of the propellant. It was found that ignition delay time was dependent on the wavelength used for detection, the method of heating, and other environmental factors. The implications of these results are discussed in relation to existing ignition theories, and recommendations are made for further study.

DD FORM 1 NOV 68 1473

Security Classification

Security Classification

14 KEY WORDS	LINK A		LINK B		LINK C	
	ROLE	WT	ROLE	WT	ROLE	WT
Composite Propellant Ignition						
Ignition Delay						
Convective Ignition						
Radiative Ignition						
Chemical Ignition						
Optical Detection of Ignition						
Fluorine Ignition						

Security Classification

Arthur D. Little, Inc.

CAMBRIDGE,
MASSACHUSETTS

CHICAGO
SAN FRANCISCO
SANTA MONICA
WASHINGTON
ATHENS
BRUSSELS
LONDON
MEXICO CITY
PARIS
RIO DE JANEIRO
TORONTO
ZURICH